An-Najah National University

Faculty of Graduate Studies

EFFECT OF HORIZONTAL COMPONENT OF EARTHQUAKE ON HANGED ROOFS LOADED WITH HEAVY WALLS

By

Motaz Mohammad Ibrahim Abu Aladas

Supervisor

Dr. Abdul-Razzaq Touqan

This Thesis is Submitted in Partial Fulfillment of the Requirements for the Degree of Master of Structural Engineering, Faculty of Graduate Studies, An-Najah National University, Nablus - Palestine.

2022

EFFECT OF HORIZONTAL COMPONENT OF EARTHQUAKE ON HANGED ROOFS LOADED WITH HEAVY WALLS

By

Motaz Mohammad Ibrahim Abu Aladas

This Thesis was Defended Successfully on 17/05/2022 and approved by

Dr. Abdul-Razzaq Touqan Supervisor	Abdul Razzaq Touqan Signature
Abdulsamee Halahla External Examiner	Signature
Monther Dwaikat Internal Examiner	Signature

Dedication

This thesis is dedicated

To the people who have supported me through this work

To My parents

To My brothers and sisters

To My teachers, colleagues and friends.

Acknowledgements

First of all, I thank God, who enabled me to do this work and helped me in it. Praise be to Him

I would like to express My thanks and appreciation to my supervisor, Dr. Abdul-Razzaq Touqan, and to all of My teachers who contributed to prepare me to complete this thesis.

Thanks to My family, colleagues and friends who have supported me

Many thanks to all of them.

Declaration

I, the undersigned, declare that I submitted the thesis entitled:

EFFECT OF HORIZONTAL COMPONENT OF EARTHQUAKE ON HANGED ROOFS LOADED WITH HEAVY WALLS

I declare that the work provided in this thesis, unless otherwise referenced, is the researcher's own work, and has not been submitted elsewhere for any other degree or qualification.

Student's Name: معتز محمد ابراهيم ابو العيس

Signature: معتز ابو العيس

Date: 17/5/2022

List of Contents

List of Tables

List of Figures

List of Appendices

EFFECT OF HORIZONTAL COMPONENT OF EARTHQUAKE ON HANGED ROOFS LOADED WITH HEAVY WALLS

By
Motaz Mohammad Ibrahim Abu Aladas
Supervisor
Dr. Abdul-Razzaq Touqan

Abstract

Background: It can be clearly seen that most of today's buildings contain cantilevers, and in most cases these cantilevers are loaded by moderate to heavy masonry loads. The effect of earthquake components on the loaded cantilevers is not clearly described in the design codes, which is a research interest. The main objective of this research is to understand the behavior of cantilevers when subjected to a horizontal earthquake component under different conditions, since the codes do not give the necessary attention to the weakness of cantilevers and their effects on the vulnerability of structures.

Methods: Some of the most sensitive properties of cantilevers were selected to study the behavior of cantilevers and their effects on the response of structures. The literature review included the investigation and collection of information on the most important factors affecting the behavior of cantilevers, such as direction, length, and loading of cantilevers. In order to study each of these parameters, a series of models with specific parameters were analyzed in the Extended 3D (Three Dimensional) Analysis of Building Systems (ETABS) software after being verified and adopted.

Results: the results of the forces and stresses in the presence of masonry have an increase of 152% for axial forces and 13.4% for shear forces and bending moments due to the horizontal component of the earthquake. On the other hand the vertical earthquake component does not have an axial effect on the cantilevered sections and the effect of axial stress due to the horizontal earthquake component on the shear capacity of sections does not exceed 2% for beams and 1% for ribs. And critical cantilever length to successive span length can reach 22% in some cases.

Conclusion: The research indicate that it's recommended to avoid an irregular structure to minimize the inherent torsion. On the other hand, a regular structure, where the center of mass coincides with the center of stiffness, may have a torsional response in some cases. Research has also shown that the horizontal earthquake component does not cause a significant decrease in shear capacity and that the vertical earthquake component is not worse than the horizontal one.

Keywords: loaded cantilever, torsional mode, horizontal earthquake component, vertical earthquake component, site seismicity.

Chapter One

Introduction and Theoretical Background

1.1 Operational definitions

Horizontal component of earthquake

Not all earthquakes are the same; many of the conditions for earthquake events affect their intensity, direction, and the components of the corresponding forces. Some of these conditions and characteristics are related to the earthquake source, some to the building, and some to the wave transmission medium.

Figure 1.A shows some conditions for earthquake events that affect the earthquake intensity and its corresponding components.

Figure 1.A

Earthquake event conditions affecting on its direction and intensity

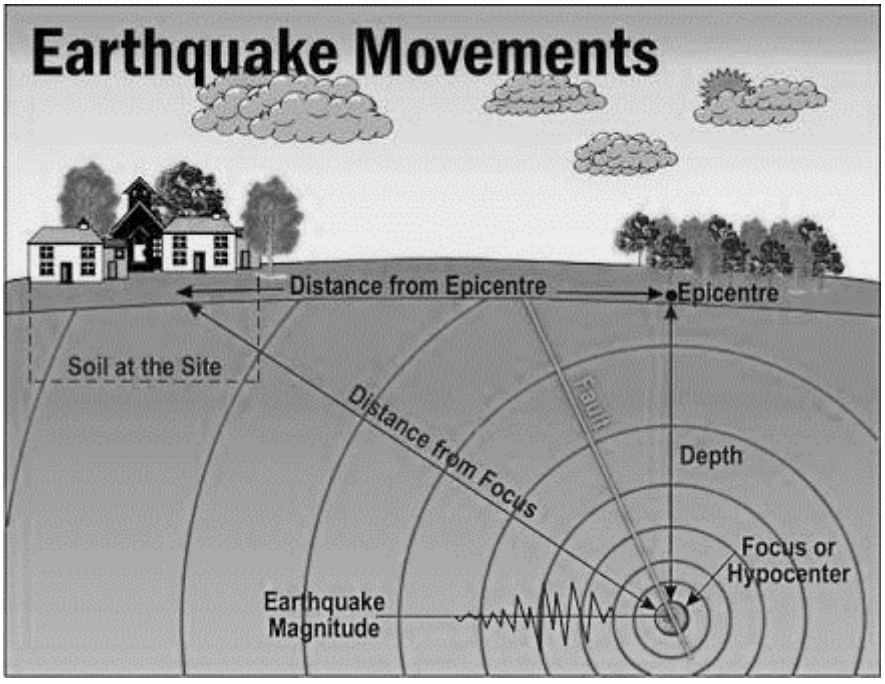

The vast majority of earthquake events are a combination of vertical and horizontal components. And the conditions and characteristics of the earthquake event greatly affect the earthquake direction and the effectiveness of the horizontal component of the earthquake.

Hanged roofs and beams

The hanged element is a beam or slab supported at only one end only and can be loaded or unloaded at its free end, as shown in Figure 1.B

Figure 1.B

Hanged roof or beam element

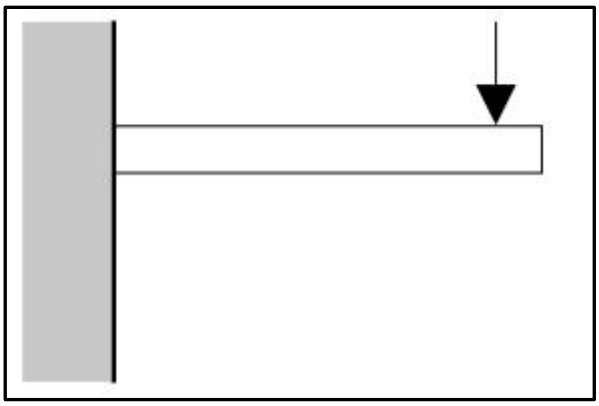

Cantilever elements are commonly used because they create an open space under the beam without the need for columns or walls. Cantilever elements have become a popular structural system and are commonly used in building construction for cantilevered elements, projections and balconies.

Cantilever beams are special, and their design can be challenging for engineers if they are long or heavily loaded, and they can deflect many times more than beams with two fixed ends and simply supported beams. These are significant differences, so cantilever deformations can be substantial and require careful design for vertical and horizontal vibration.

Table 1.A shows the relationship between the results for shear force, bending moment, and deflection due to concentrated load at the ends of cantilever beam and the results for simply supported beams due to concentrated load at midspan, with the length of the cantilever selected as half the simply supported length.

Table 1.A

Cantilever to simply supported beams results ratio

System	Length	Shear_max	Moment_max	Delta_max
Simply supported	L	WL/2	$WL^2/8$	$5WL^4/384EI$
Cantilever	L/2	W(L/2)	$W(L/2)^2/2$	$W(L/2)^4/8EI$
cantilever to simply supported results ratio		1	1	0.6

The inelastic behavior was neglected because it is limited by shape factor, the cantilever element carries a single plastic hinge before collapse, and there is no possibility of redistributing the loads.

The vertical earthquake component was only conceptually presented and investigated in the last chapter and applied as a percentage of the horizontal earthquake component for comparison purposes.

1.2 Literature review

The behavior of buildings subjected to the forces of an earthquake depends on the distribution of their mass and stiffness in horizontal and vertical planes. In such buildings, damage from earthquake shaking usually occurs at the weak points of the structure. In some cases, these weak points may be due to discontinuities in stiffness, strength, or mass between adjacent floors. The presence of irregularities in reinforced concrete buildings (RC) increases seismic vulnerability. The American Society of Civil Engineers, in its Minimum Design Loads and Associated Criteria for Buildings and Other Structures (ASCE7-16) manual, divides irregularities into vertical and horizontal irregularities.

Cantilevers are a form of irregular massing common in urban environments to increase floor plan dimensions and provide space for balconies (Hasan Huesnue KORKMAZ, 2018).

The problems related to cantilevers (Ozmen and Unay 2007; Inel et al., 2008) can be summarized as that they lead to torsional irregularities and their lateral stiffness is different from that of the floors below or above. Or the center of mass of the building is shifted upward and away from the center of stiffness. Or they experience critical displacements during earthquakes that can lead to partial collapse.

The behavior of cantilevers differs depending on the load and geometry. The loads applied to the cantilever depend on its use, its location, the presence of walls at the end of the cantilever, and the geometry and materials of these walls. (Goutam Mondal and Solomon Tesfamariam, 2013) studied the effect of an infill wall supported by a cantilever on the collapse mechanism of a RC frame under lateral loading and found that as the thickness of the wall increases, the tendency for a soft story mechanism to occur increases. (D. H. HODGES, 2001) explained and differentiated the effect of cantilever length, section dimensions and cantilever peak load on the sequence of modes. (Özgür Yurdakul- Burak Duran- Onur Tunaboyu· Özgür Avşar, 2020) also explain how the external infills above the overhangs become more vulnerable to in-plane and out-of-plane actions.

(D ZHOU, 1997) differentiates and explains that when the excitation frequency of the base motion is equal to the natural frequencies of the beam, resonance occurs and the amplitude of the beam is infinite, so that the natural frequencies of the structure can be calculated from the relations by the method of nonlinear algebraic equation search roots.

(J.-J. WU AND A. R. WHITTAKER, 1999) found that the influence on the dynamic properties of a uniform beam by the action of a concentrated load is much greater than that by distributed loads.

1.3 A problem statement

A major objective in the seismic design of structures is to ensure that the structure will perform acceptably when subjected to ground motions of various directions, intensities, and probabilities of occurrence during its life.

In some buildings, overhangs are placed for architectural reasons, which play an important role in earthquake damage to these buildings. On the other hand, the modal response of the structure is strongly influenced by open and closed overhangs, such as balconies, and the infill materials used in these overhangs.

1.4 Aims of study

The study aims to investigate the effect of the horizontal component of earthquakes on buildings with cantilever systems and the effect of the associated cantilever parameters such as cantilever length, loads and cantilever directions on the dynamic behavior of the structure when subjected to the same earthquake component.

The research focused on the following:

- The relationship between the cantilever parameters and the sequence of modes and the response of the structure, Figure 1.C shows some of modes shapes due to earthquake action.

Figure 1.C

Some of modes shapes due to earthquake action

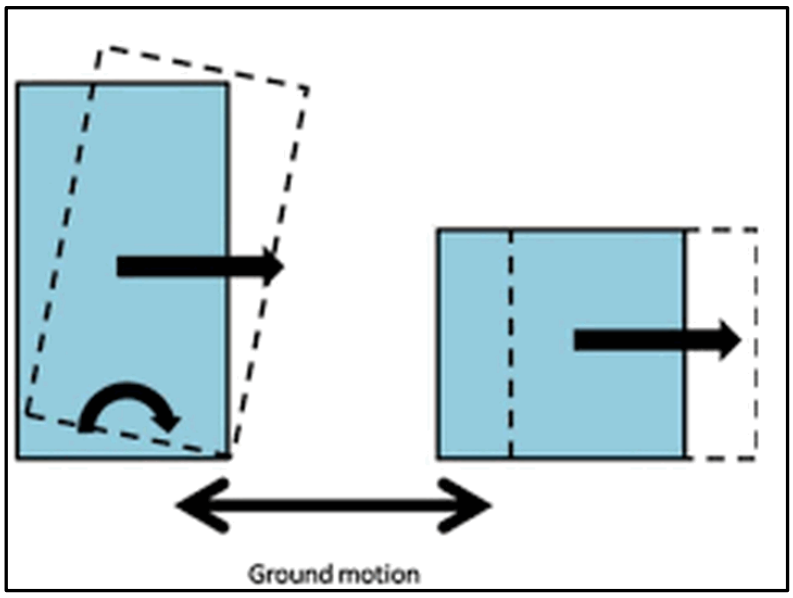

- The effect of the horizontal component of the earthquake on the capacity of cantilevers for the other force components, **Figure** 1.D shows the principle stresses in two and three directions and the combination of tension and compression stresses.

Figure 1.D

Principle stresses in two and three directions and the combination of tension and compression stresses

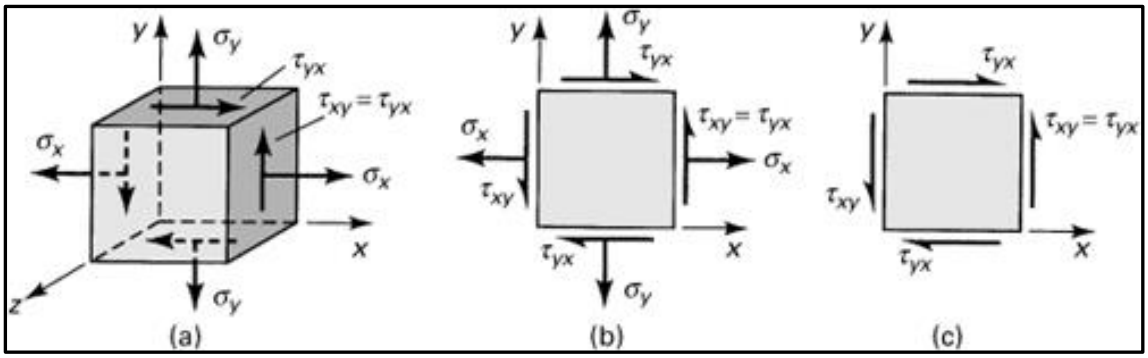

- The effect of site seismicity and building location on cantilever beam forces and stresses due to the horizontal earthquake component, Figure 1.E shows Waves formation in hard rock and soft soil sites.

Figure 1.E

Waves formation in hard rock and soft soil sites

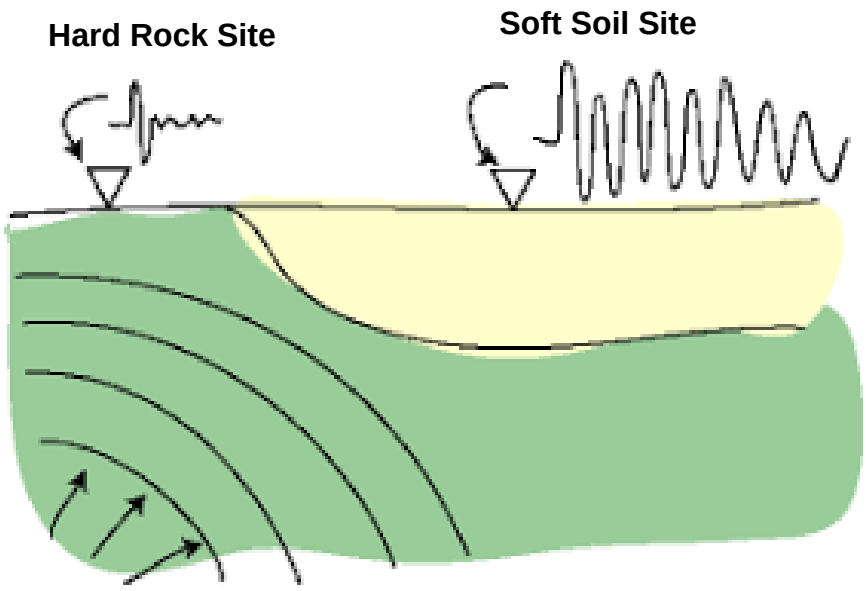

1.5 The importance of study

The importance of the study was characterized by creating a qualified sense of the performance of buildings with cantilevers and estimated the effect of changing the cantilever parameters.

Chapter Two
Methodology

2.1 Analysis plan

The analysis began by gathering information on the study topics from codes and previous researches, then using the collected data to determine the parameters to be studied and analyzed.

The next step was to select structures with common dimensions and properties in a simple form to minimize sources of error and simplify the verification calculations. Reinforced concrete was selected as the structural material, with same properties for all analyzed structures.

In the first part, the effects of the cantilever directions and distributions on the sequence of modes, torsional irregularity and torsional behavior were investigated. The distribution and direction of the cantilevers play an important role in the behavior of the structure under earthquake action. When the mass and loads of the cantilevers are included in the total mass of the structure, the changes in the distribution and geometry of the cantilevers change the location of the center of mass of the whole structure and may cause additional irregularities, eccentricities, and torsional behavior.

In the second part, the effect of cantilever length and load on the sequence of modes is studied by taking four sets of four different models with different cantilever lengths, each set representing a different architectural pattern for the cantilevers in terms of their exposed load subjected to a uniform superimposed dead load in addition to a line of superimposed dead load at the end of the cantilevers.

The third part discussed the effect of cantilever length and load on shear capacity. The ability of sections to resist shear forces under only vertical static loads is compared with their shear capacity after a horizontal earthquake component is added. Tensile forces are known to have a significant effect on reducing the shear strength of the section. In this chapter, the effect of axial tension on the shear strength of loaded cantilever elements is investigated. This problem does not usually arise in the investigation and design of structures designed for gravity loads only.

However, in a horizontal earthquake, the capacity of the structure to resist shear forces must be verified when tensile forces parallel to the cross-sections of beams and slabs result from horizontal earthquake forces.

In the last part, the effects of location seismicity on the behavior of loaded and unloaded cantilevers subjected to horizontal and vertical earthquake components were studied. Site seismicity plays a very important role in characterizing seismic ground motions, as they can greatly amplify seismic motions before they reach structures. The high level of amplification caused by the nature of the site means that the site effect cannot be neglected in engineering practice.

All real ground motions contain three orthogonal components. For most structures, only the response to the horizontal components of ground shaking need be considered. However, for structures defined as sensitive to vertical earthquake effects, consideration of the vertical components is required. ASCE7-16 classifies buildings near fault locations and buildings with cantilevers as sensitive to vertical earthquake effects.

At the end of the study, the results should be analyzed to obtain curves or percentages that can guide designers in the use of cantilevers and then write a conclusion.

2.2 Structure description

The structures studied were selected as a simple structure with a typical grid, and the dimensions of the structural elements were chosen to meet the design requirements for dead and live loads.

The structures selected to be a structure of reinforced concrete with 24MPa concrete compressive strength 25kN/m3 unit weight and elastic modulus of 23025 MPa. The weight of the structure, in addition to the imposed dead load of 4.26 kN/m2 for the models with two ribbed slabs and 4.55 kN/m2 for the models with one ribbed slab, is used as a mass source to determine the seismic load. The calculations of the applied loads were explained in Appendix B for the masonry wall load and the dead load applied to the slabs (SID).

The response spectrum curves were generated using realistic and commonly used seismic data in the city of Nablus with a design spectral acceleration SDS and SD1 of 0.6 and 0.405, respectively, for the horizontal components.

Each of the modeled structures consists of a floor, unless otherwise specified, with a height of 3.25 meters and fixed column bases, the columns being chosen as square columns of 30 cm. The slab is a two way ribbed slab with a thickness of 25 cm. The beams have a width of 60 cm or 40 cm and a depth of 25 cm, and the cantilevered end beams are 20 cm width and 25 cm depth.

In the first set of models used to study the effect of cantilever directions on the vulnerability of the structure, the slab system was selected as a two way ribbed slab and the effect of wall load at the end of the cantilever was neglected.

The cantilever length was set at 2 m, and the eccentricity created by the single cantilever in a given direction-no opposing cantilever-was 1 m, and the weight of the columns was neglected to simplify the calculations.

Five models with different cantilever directions, including the single cantilever model, have an eccentricity of one meter in the X direction, as shown in Figure 2.A.

Figure 2.A

Single cantilever model

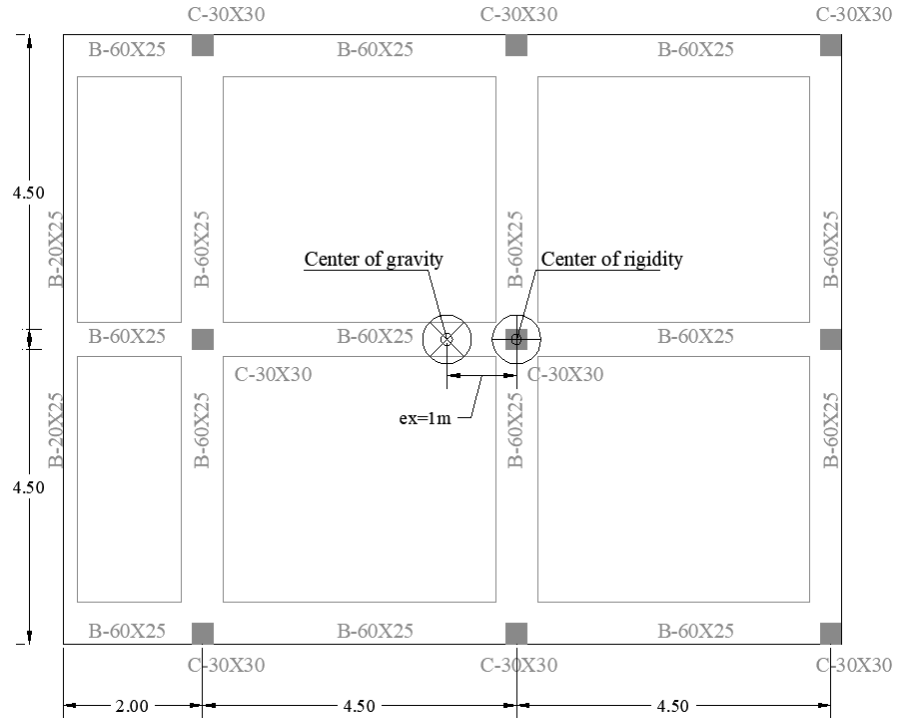

The double cantilever model in the same direction has no eccentricity, as shown in Figure 2.B.

Figure 2.B

Double cantilever in same direction model

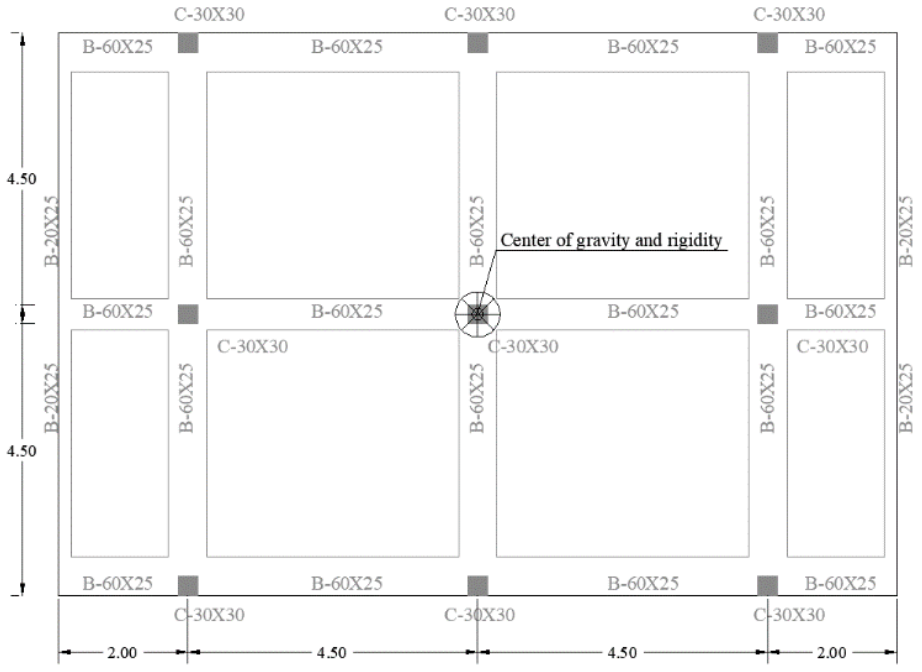

The model of the double cantilever in different directions has an eccentricity of 1 m in the X and Y directions, as shown in Figure 2.C

Figure 2.C

Double cantilever in different directions model

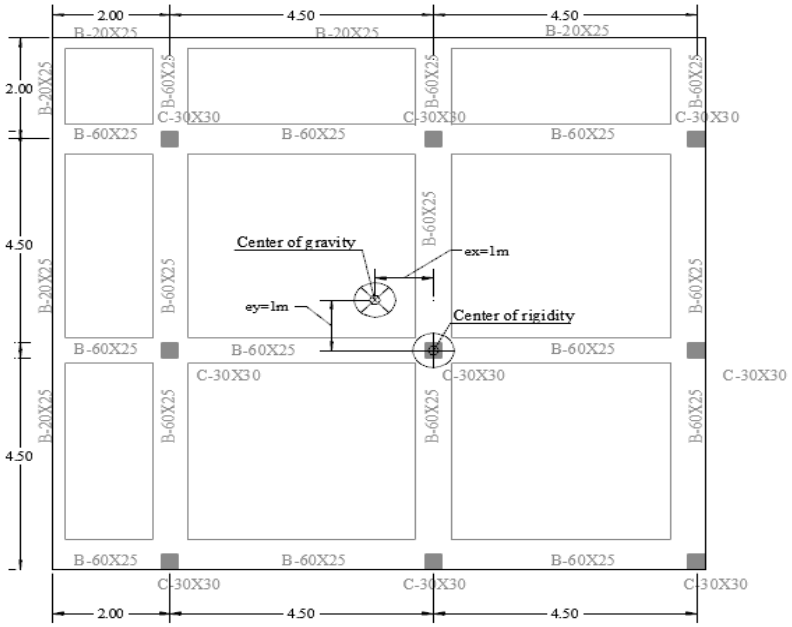

The model of the triple cantilever has an eccentricity of one meter in the Y direction, as shown in Figure 2.D

Figure 2.D

Triple cantilever model

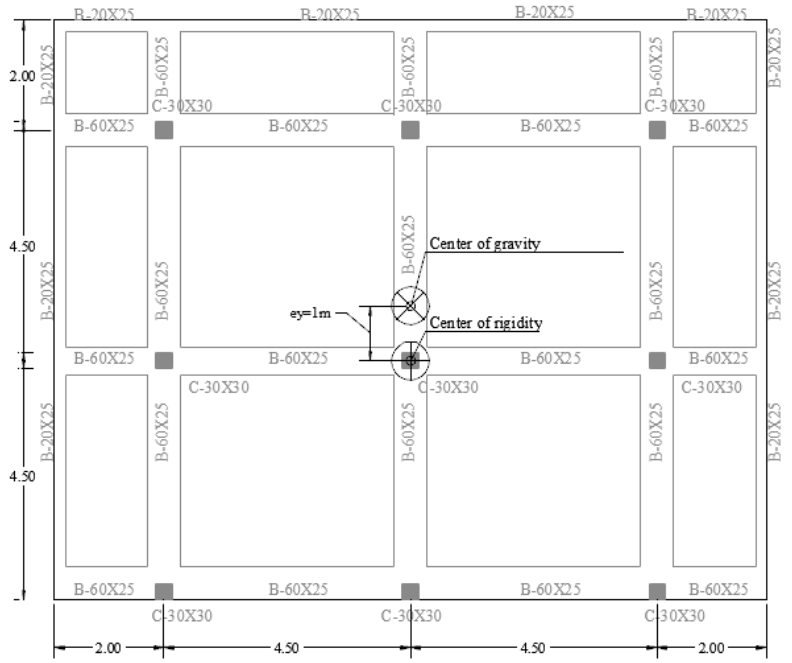

And the model with fourfold cantilevers, as shown in Figure 2.E

Figure 2.E

Fourfold cantilever model

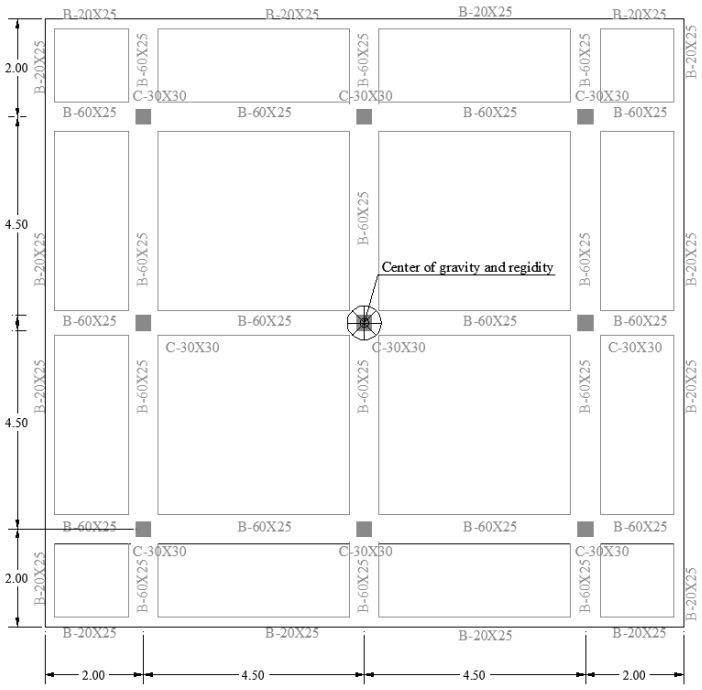

In the second set of models used to study the effect of cantilever length and loading on the sequence of modes, a single panel with a width of 4.5 m contains two interior continuous spans of 4.5 m connected at each end by cantilevers of different lengths (0.5 m, 1 m, 1.5 m, and 2 m). The slab was selected as a one way ribbed slab, as shown in Figure 2.F.

Figure 2.F

Plan dimensions and layout

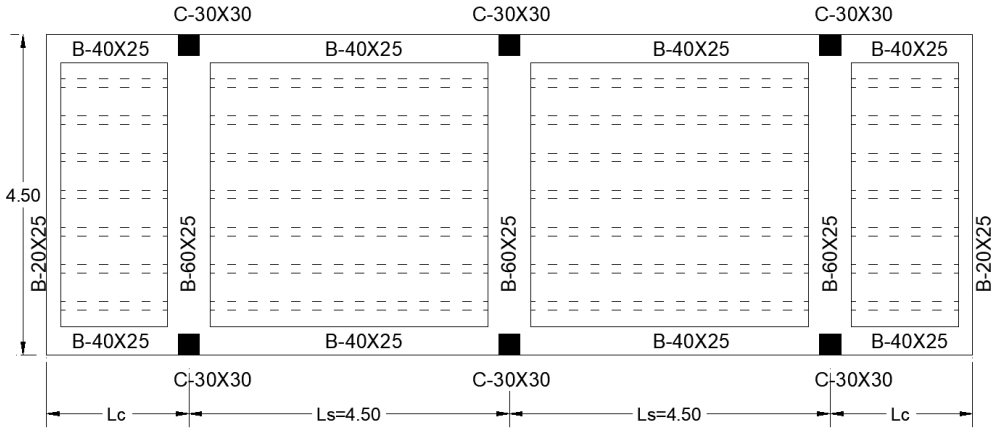

Figure 2.G shows the mass source in the dynamic analysis:

Figure 2.G

Models dimensions and loads distribution for analyzed models

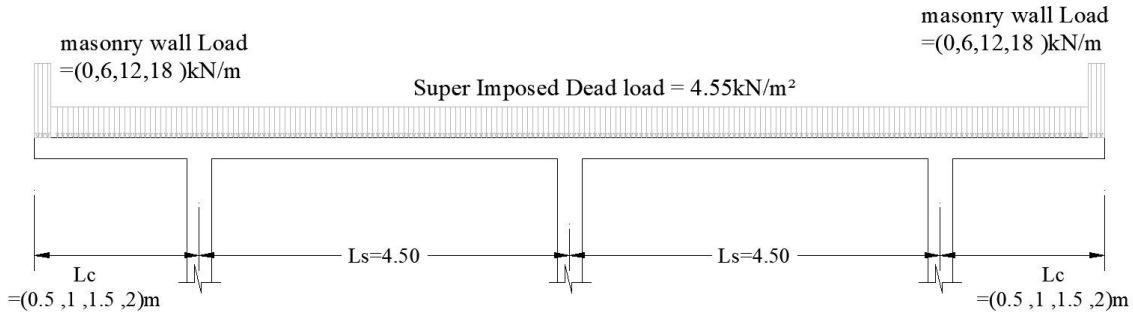

In the third part, which examines the effect of cantilever length and load on shear capacity, the model set used in the second part was used again, but with three stories.

In the fourth model set, used to study the effects of location on the behavior of loaded and unloaded cantilevers under earthquake components in different directions, a slab 4.5 m wide contains two interior continuous spans of 4.5 m connected to cantilevers 2 m long at each end. The slab selected as two way ribbed slab, as shown in Figure 2.H.

Figure 2.H:

Structural plan layout

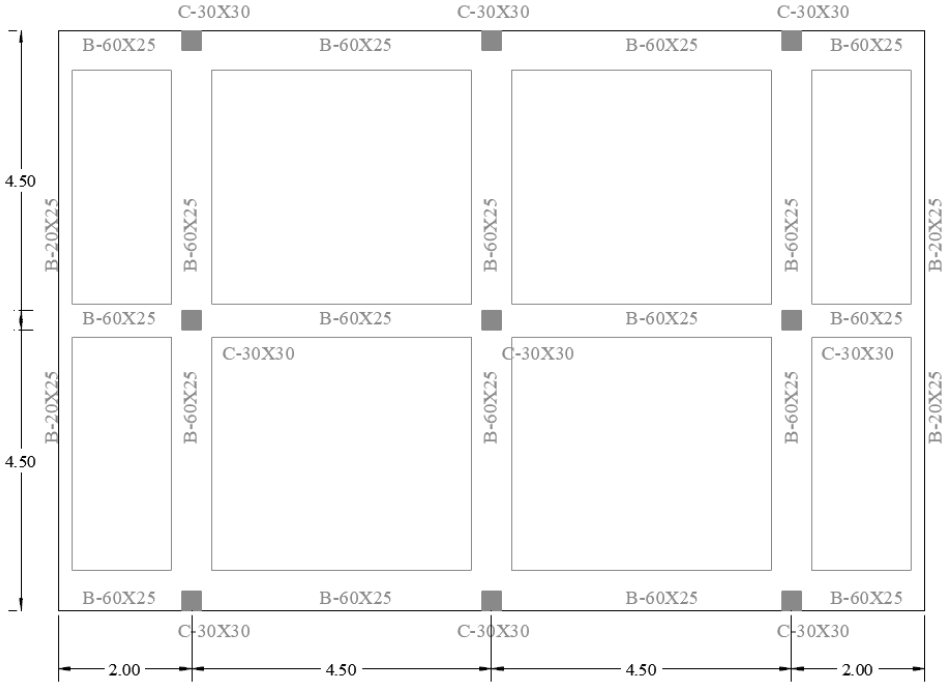

2.3 Structure modeling

The modal response spectrum analysis method was chosen for the seismic analysis because it's a relatively simple and fast method, and the effects of nonlinearity weren't considered in this study.

The structure was modeled with different modeling conditions, each representing different Palestinian cities (Jericho, Nablus, Hebron, and Beer Saba), and the base accelerations (Z) were (0.3, 0.2, 0.15, and 0.075, respectively), the maximum short period (Sms) earthquake spectral response parameters considered were (1.2, 0.9, 0.8, and 0.4, respectively), the maximum considered parameters for spectral earthquake response acceleration for 1s period (Sm1) were (1, 0.6, 0.5, and 0.3, respectively), the importance factor was set to 1, and the bearing capacity of soil is 150 kN/m2 in each city.

Based on the previous information, the acceleration parameters of the design spectrum for the horizontal component in each city were calculated as shown in Table 2.A, and the calculation steps were explained in Appendix C.

Table 2.A

Design spectrum parameters for horizontal earthquake component in the four cities

City	SDs	SD1
Jericho	0.8	0.6
Nablus	0.6	0.4
Hebron	0.5	0.3
Beer Saba	0.3	0.2

The vertical curves of the response spectrum were chosen to be constant, with the peak ground acceleration (PGA) equal to half of the PGA in the horizontal curves of the response spectrum; Table 2.B shows the (PGA/g) values in each city for horizontal and vertical components.

Table 2.B

(PGA/g) for horizontal and vertical components

	Horizontal PGA/g	**vertical PGA/g**
Jericho	0.32	0.16
Nablus	0.24	0.12
Hebron	0.20	0.10
Beer Saba	0.12	0.06

2.4 Computer program verification

Before adopting a structural design program, there is an inevitable step, which is the results and outputs verification. Whether the objectives are commercial or scientific, it is necessary to verify that the program results are compatible with manual calculations or laboratory results. In this thesis, the program ETABS V18.0.0 is used after its results and outputs have been verified in this chapter according to the verification criteria of Computers and Structures, Inc. (CSI). Verification is performed for all required program results, including static and dynamic analysis.

Acceptance Criteria

The comparison of the results of the ETABS verification model with the results of the manual calculations is typically called exact if the difference between the ETABS results and the results of the manual calculations is zero. On the other hand, the difference is acceptable if the percentage difference between the ETABS results and the results of the manual calculations is not more than (5%) for force, moment and displacement values, and the percentage difference is less than (10%) for the values of internal forces and stresses, and the difference is called unacceptable if the percentage difference is more than the previously mentioned limits

The equation below shows the formula for the percent difference as explained in **(Computers & Structures, Inc verification manual, 2016)**.

$$\text{Percent Difference} = 100 * \left(\frac{\text{Etabs result}}{\text{independent result}} - 1\right) \quad (2.1)$$

Structure Description

A reinforced concrete structure made of a single slab 4.5 m wide contains two interior continuous spans, each 4.5 m long, connected at each end by 2 m cantilevers, as shown in Figure 2.I.

The system is not practical in our country, but it is used in other countries and it's used to match the analyzed models roof system, the beams were neglected when the model with beams is not easy to be verified manually.

The roof of the verification model was analyzed as a rigid diaphragm for the verification of the modal results verification (period and frequency) and as a semi rigid diaphragm for the verification of the forces and stresses.

Figure 2.I

Verification model floor plan

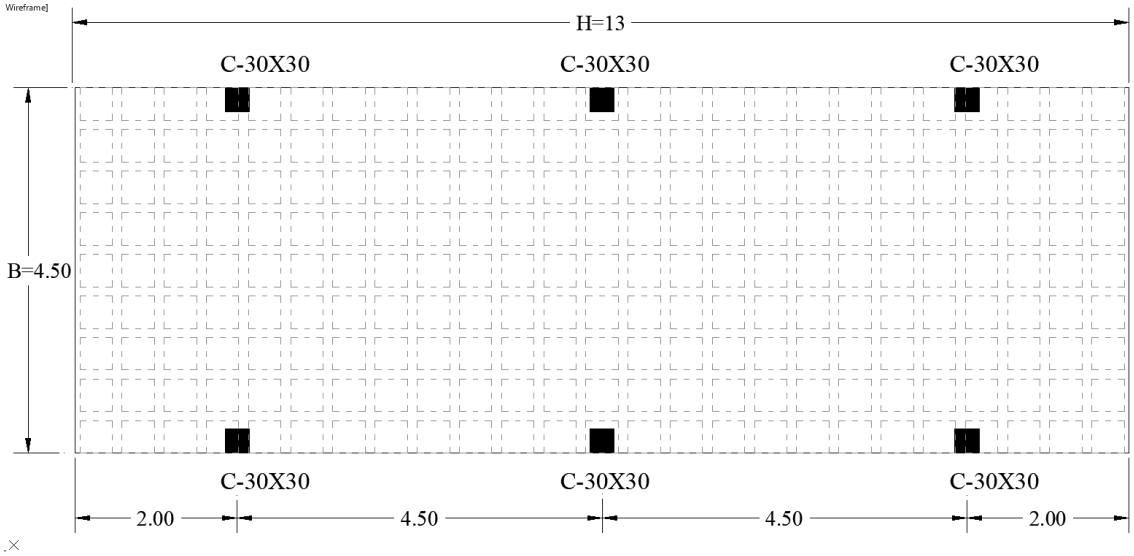

The structure consists of one floor with a height of 3.25 m and fixed columns, as shown in Figure 2.J.

Figure 2.J

Verification model elevation and dimensions.

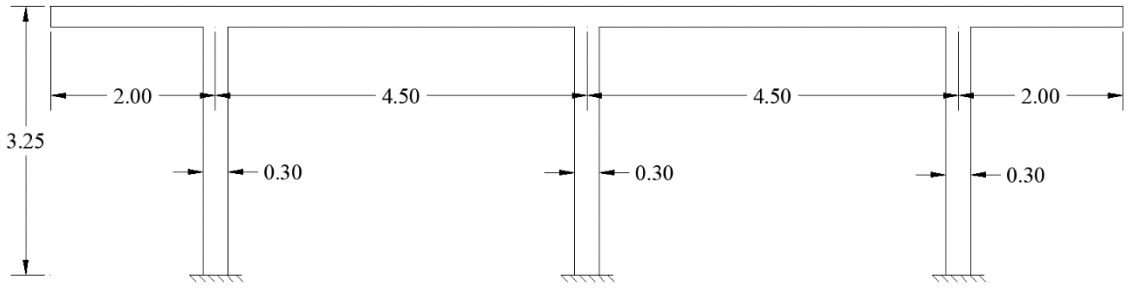

The column sections were determined as 30X30 cm, and the slab was chosen as a two way ribbed slab with a thickness of 25 cm without beams as shown in Figure 2.K.

Figure 2.K

Columns and slab sections for verification model

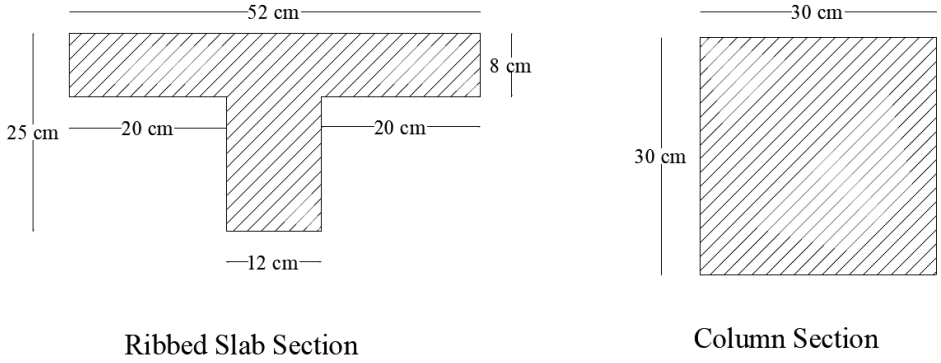

Ribbed Slab Section

Column Section

Manual calculations

In the first step, structure weight (D) and the super imposed dead load (SID) are calculated:

$$\text{Slab weight} = \left(1 - \frac{0.4 * 0.4 * 0.17}{0.25 * 0.52 * 0.52}\right) 4.5 * 13 * 0.25 * 25 = 218.51 \text{ kN}$$

$$\text{Columns Weight} = 0.3 * 0.3 * 6 * 3.25 * 25 = 43.875\text{kN}$$

$$\text{D} = 269.54 + 43.875 = 262.38 \text{ kN}$$

$$SID = 4.5 * 13 * 3.9 = 228.15 \text{ kN}$$

In the next step, modal periods, frequencies, and modes directions were calculated:

For buildings with rigid floors (diaphragms), where the center of gravity and the center of stiffness are the same and there are no irregularities in the structure and the modes are decoupled, the mass and stiffness matrices can be calculated as in Equation (2.2):

$$[M] = \begin{bmatrix} m_u & 0 & 0 \\ 0 & m_v & 0 \\ 0 & 0 & m_\theta \end{bmatrix}, [K] = \begin{bmatrix} k_u & 0 & 0 \\ 0 & k_v & 0 \\ 0 & 0 & k_\theta \end{bmatrix} \quad (2.2)$$

M_u and m_v are the translational mass coefficients,

$$m_u = m_v = \frac{262.38 + 228.15}{9.81} = 50 \text{ ton}$$

and $m_\vartheta =$ The mass polar moment of inertia

$$m_\vartheta = m * \left(\frac{B^2}{12} + \frac{H^2}{12}\right) \quad (2.3)$$

Using equation (2.3), where B=4.5m and H=13m as shown in Figure 2.L.

$$m_\vartheta = 50 * \left(\frac{4.5^2}{12} + \frac{13^2}{12}\right) = 786 \text{ ton.m}^2$$

And the next are the vertical mass and stiffness coefficients

$$m_z = 50\text{ton}$$

$$K_z = n * \frac{E * A}{L} \quad (2.4)$$

Using equation (2.4)

$$K_z = 6 * 23025 * \frac{0.3^2}{3.25} * 1000 = 3825.7 * \frac{10^3 \text{kN}}{m}$$

Where m_z is the vertical translation mass coefficient and K_z is the axial stiffness coefficient.

The mass matrix based on equation (2.2): $[M] = \begin{bmatrix} 50 & 0 & 0 \\ 0 & 50 & 0 \\ 0 & 0 & 786 \end{bmatrix}$

Figure 2.L

Floor plan shows center of gravity and center of stiffness in addition to H & B definition.

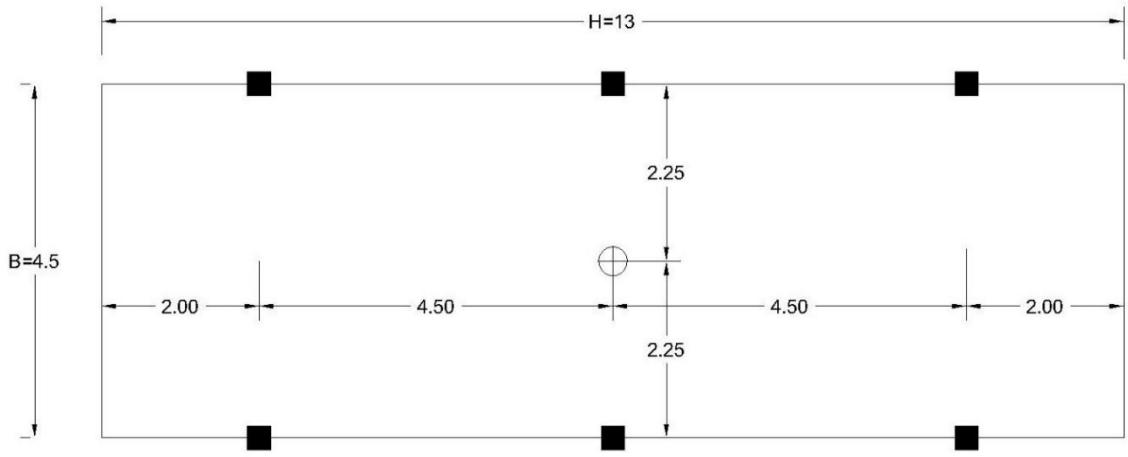

The next step is calculating stiffness matrix starting from column stiffness Kc:

$$K_c = \frac{12EI}{L^3} \tag{2.5}$$

Using equation (2.5)

$$K_c = \frac{12 * 23024 * \frac{0.3^4}{12}}{3.25^3} * 1000 = \frac{5432.94\text{kN}}{\text{m}}$$

k_u and k_v are the translational stiffness coefficients

$$K_u = K_v = 6 * K_c = 6 * 5432.94 = \frac{32597.61\text{kN}}{\text{m}}$$

And k_ϑ is the rotational stiffness coefficient, Figure 2.M shows the rotational stiffness components for each column.

$$K_\vartheta = \sum_{i=1}^{n} Kc_i * r_i^2 \tag{2.6}$$

Where r_i is the perpendicular distance between stiffness component and center of rigidity.

Based on equation (2.6):

$$K_\vartheta = K_c * (4 * 4.5^2 + 6 * 2.25^2) = 605093\text{kN}.\frac{m^2}{m}$$

The stiffness matrix is based on equation (2.2):

$$[K] = \begin{bmatrix} 32597.61 & 0 & 0 \\ 0 & 32597.61 & 0 \\ 0 & 0 & 605093 \end{bmatrix}$$

Figure 2.M

Rotational Stiffness components

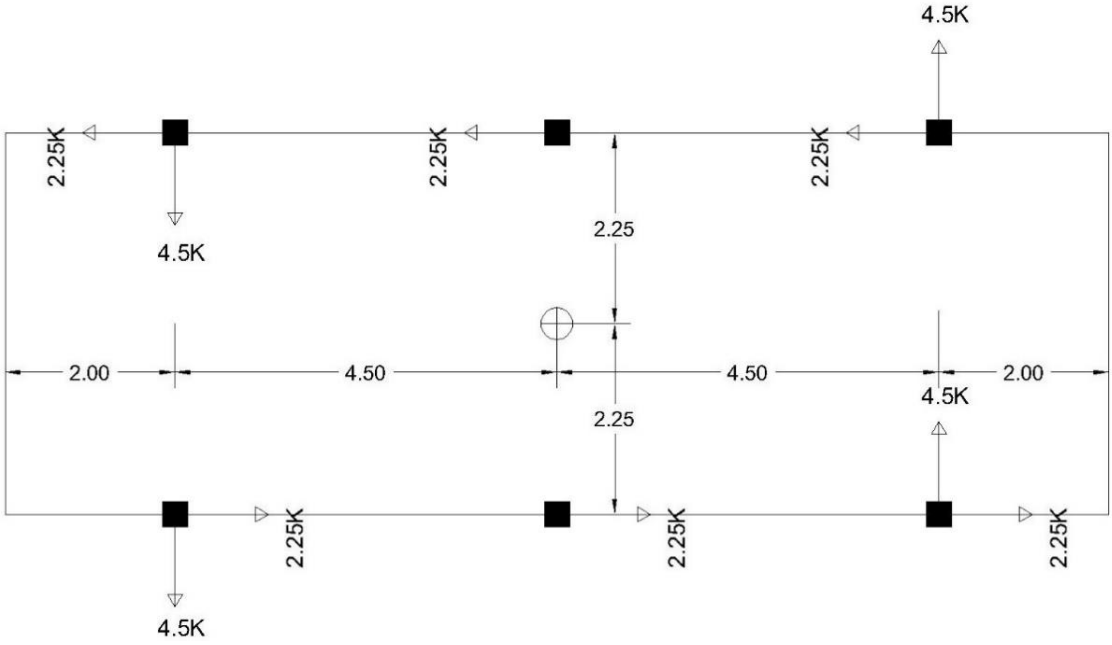

When the mass and stiffness matrices are known then we can calculate the natural frequencies and periods for the first three modes:

Eigenvalue formulation yields

$$[K - \omega^2 * M] = \{0\} \qquad (2.7)$$

Frequency equation is given as:

$$\begin{bmatrix} (k_u - \omega^2 * m_u) & 0 & 0 \\ 0 & (k_v - \omega^2 * m_v) & 0 \\ 0 & 0 & (k_\theta - \omega^2 * m_\theta) \end{bmatrix} = 0$$

The results are three independent equations of the form $k_i - \omega_i^2 * m_i = 0$, which yields three frequencies:

$$\omega_i = \sqrt{\frac{K_i}{m_i}} \tag{2.8}$$

Using Equation (2.8)

$$\omega_u = \omega_v = \sqrt{\frac{32597.6}{50}} = 25.57 \frac{rad}{S}$$

$$\omega_\vartheta = \sqrt{\frac{K_\vartheta}{m_\vartheta}} \tag{2.9}$$

Using Equation (2.9)

$$\omega_\vartheta = \sqrt{\frac{605093}{786}} = 27.75 \frac{rad}{S}$$

The natural frequency in vertical direction can be calculated conceptually with same idea:

Using Equation (2.8)

$$\omega_z = \sqrt{\frac{3825.7 * 10^3}{50}} = 277.055 \frac{rad}{S}$$

$$f \tag{2.10}$$

Using Equation (2.10)

$$T_u = T_v = 2\pi * \sqrt{\frac{50}{32597.6}} = 0.246\ S$$

$$T_{\vartheta} = 2\pi * \sqrt{\frac{Ip}{K_{\vartheta}}} \quad (2.11)$$

Using Equation (2.11)

$$T_{\vartheta} = 2\pi * \sqrt{\frac{786}{6050.93 * 10^3}} = 0.226\ S$$

The natural period in vertical direction can be calculated conceptually by using Equation (2.10):

$$T_z = 2\pi * \sqrt{\frac{50}{3825.7*10^3}} = 0.023\ S$$

To calculate stresses and forces in frames and shells, we must first find the pseudo-acceleration from the applied response spectrum curve at the natural period related to the same direction:

$$Sa_x = 9.81 * 0.6 = 5.886 \left(\frac{m}{S^2}\right)$$

$$Sa_y = 9.81 * 0.6 = 5.886 \left(\frac{m}{S^2}\right)$$

$$Sa_z = 9.81 * 0.12 = 1.18 \left(\frac{m}{S^2}\right)$$

In this model, three different earthquake components were applied to the structure, the first is a horizontal component in the X direction, the second is a horizontal component in the Y direction with an eccentricity of 1 metre, which is 7.7% and greater than the code recommendation, and the third is a vertical component in the Z direction. To calculate the lateral drift at the floor level we need to calculate the lumped mass at the same level, in this case the lumped mass at the floor level equal to the total mass of the structure minus half of the column masses.

The lateral drift due to the horizontal component of the earthquake in the X direction is calculated as follows:

$$Sd_i = \frac{Sa_i}{\omega_i^2} \quad (2.12)$$

$$m_u = 50 - \left(\frac{\left(6 * 0.3^2 * 25 * \frac{3.25}{2}\right)}{9.81} \right) = 47.6 \text{ ton}$$

Using Equation (2.8)

$$\omega_u = \sqrt{\frac{32597.6}{47.6}} = 26.17 \frac{\text{rad}}{S}$$

Using Equation (2.12)

$$Sd_x = \frac{5.886}{26.17^2} = 0.0086 \text{ m}$$

The lateral drift due to the horizontal component of the earthquake in the Y direction with an eccentricity of 1 meter is calculated as follows:

$$m_v = 50 - \left(\frac{\left(6 * 0.3^2 * 25 * \frac{3.25}{2}\right)}{9.81} \right) = 47.6 \text{ ton}$$

Using Equation (2.8)

$$\omega_v = \sqrt{\frac{32597.6}{47.6}} = 26.17 \frac{\text{rad}}{S}$$

Using Equation (2.12)

$$Sd_y = \frac{5.886}{26.17^2} = 0.0086\text{m}$$

$$V_i = Sd_i * K_i \quad (2.13)$$

Using Equation (2.13)

$$V_y = 0.0086 * 32597.6 = 280.34 \text{ kN}$$

And the rotation about the Z axis due to the horizontal component of the earthquake in the Y direction with an eccentricity of 1 meter is calculated as follows:

$$M = e * V_i \tag{2.14}$$

Using Equation (2.14)

$M = 1 * 280.34 = 280.34$ kN. m

$$R_\vartheta = \frac{M}{K_\vartheta} \tag{2.15}$$

Using Equation (2.15)

$$R_\vartheta = \frac{M}{K_\vartheta} = \frac{280.34}{605093} = 46.33 * 10^{-5} rad$$

The upward drift due to vertical component of earthquake in Z-direction calculated using Equation (2.12):

$$Sd_z = \frac{1.18}{277.055^2} = 1.54 * 10^{-5} \text{ m}$$

The base shear bending moment due to horizontal earthquake component in X direction can be calculated Using Equation (2.13):

$V_{x\,total} = 0.0086 * 32597.6 = 280.34$ kN

The shear force in each column:

$$V_{i\,column} = \frac{V_{i\,total}}{\#columns} \tag{2.16}$$

Using Equation (2.16)

$$V_{column} = \frac{280.34}{6} = 46.72 \text{ kN}$$

The total bending moment is:

$$M_{total_i} = V_i * H_{story} \quad (2.17)$$

Using Equation (2.17)

$M_{total_X} = 280.34 * 3.25 = 911.1\ \text{kN.m}$

The bending moment in each column is:

$$M_{column_i} = V_{column_i} * \frac{H_{story}}{2} \quad (2.18)$$

Using Equation (2.18)

$M_{column_X} = 48.89 * \frac{3.25}{2} = 75.92\ \text{kN.m}$

The base shear bending moment due to the horizontal earthquake component in the Y direction with an eccentricity of 1 m can be calculated using equations (2.13) and (2.16) respectively:

$V_{total_y} = 0.0086 * 32597.6 = 280.34\ \text{kN}$

$V_{column_y} = \frac{280.34}{6} = 46.72$

General Shear force formula:

$$V_{yi} = \frac{K_{yi}}{\sum K_{yi}} * V_y \pm K_{yi} * \frac{X_i}{K_\theta} * V_y * e \quad (2.19)$$

Using Equation (2.19)

$V_{y1} = \frac{1}{3} * 280.34 + 2 * 5432.94 * \frac{4.5}{605093} * 280.34 * 1 = 116.1\text{kN}$

$V_{column1} = \frac{116.1}{2} = 58.05\text{kN}$

$V_{y2} = \frac{1}{3} * 280.34 + 2 * 5432.94 * \frac{0}{605093} * 280.34 * 1 = 93.47\text{kN}$

$V_{column2} = \frac{93.47}{2} = 46.73\text{kN}$

$$V_{y3} = \frac{1}{3} * 280.34 - 2 * 5432.94 * \frac{4.5}{605093} * 280.34 * 1 = 70.79\text{kN}$$

$$V_{column3} = \frac{70.79}{2} = 35.4\text{kN}$$

And the bending moment is:

$$M_{total_y} = 280.34 * 3.25 = 911.1$$

$$M_{column1} = 58.05 * \frac{3.25}{2} = 94.33$$

$$M_{column2} = 46.73 * \frac{3.25}{2} = 75.94$$

$$M_{column3} = 35.4 * \frac{3.25}{2} = 57.5$$

The axial load due to the horizontal earthquake component in the X-direction can be calculated using the free body shown in Figure 2.N:

Figure 2.N

Free body diagram for the half of structure.

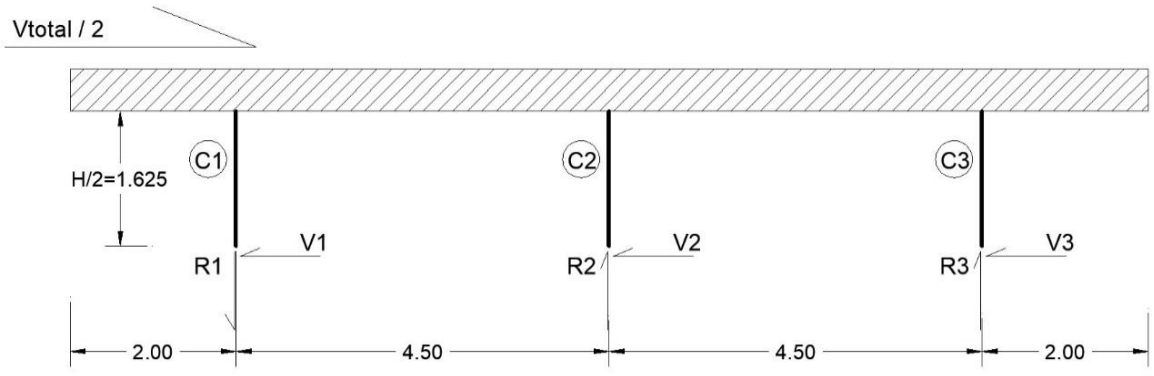

R1=-R3

Σ moments at mid of column C2

$$\Sigma M = \frac{V_{total}}{2} * \frac{H_{story}}{2} - 2R_{1,3} * L_{Span} = \frac{280.34}{2} * \frac{3.25}{2} - 2 * R_{1,3} * 4.5 = 0$$

$R_{1,3} = 25.3$ kN and $R_2 = 0$

The axial load due to horizontal earthquake component in Y direction with eccentricity of 1 meter can be calculated as the following:

$$P_{Ci} = 2 * V_{Ci} * \frac{\frac{H_{story}}{2}}{L_{span}} \quad (2.20)$$

Using Equation (2.20)

$$P_{C1,3} = 2 * 58.05 * \frac{\frac{3.25}{2}}{4.5} = 41.92$$

$$P_{C2} = 2 * 46.73 * \frac{\frac{3.25}{2}}{4.5} = 33.75$$

The axial load due to vertical earthquake component in Z direction is:

$$P_{total} = Sa * m = 1.18 * 47.6 = 56.17$$

$$P_{col} = \frac{56.17}{6} = 9.36$$

Now we can calculate the forces and stresses in the shells due to each earthquake component. The following figures show the forces and stresses due to the horizontal earthquake component in the X direction. To simplify the calculation of the axial forces, the developed stresses due to each plate were analyzed separately, as shown below:

Axial force for each 1 meter square:

$$P = \frac{(1 * 1) * (3 + 0.97 * 0.19 * 25)}{9.81} * (0.6 * 9.81) = 4.565$$

Axial force centered in cantilever:

$$P = \frac{(4.5 * 2) * (3 + 0.97 * 0.19 * 25)}{9.81} * (0.6 * 9.81) = 41.08$$

Axial force centered in continuous span:

$$P = \frac{(4.5 * 4.5) * (3 + 0.97 * 0.19 * 25)}{9.81} * (0.6 * 9.81) = 92.43$$

Then combined to each other to get the axial force diagram as shown in Figure 2.P:

Figure 2.O

Resultant axial forces resultant in the floor and columns, arrows plot

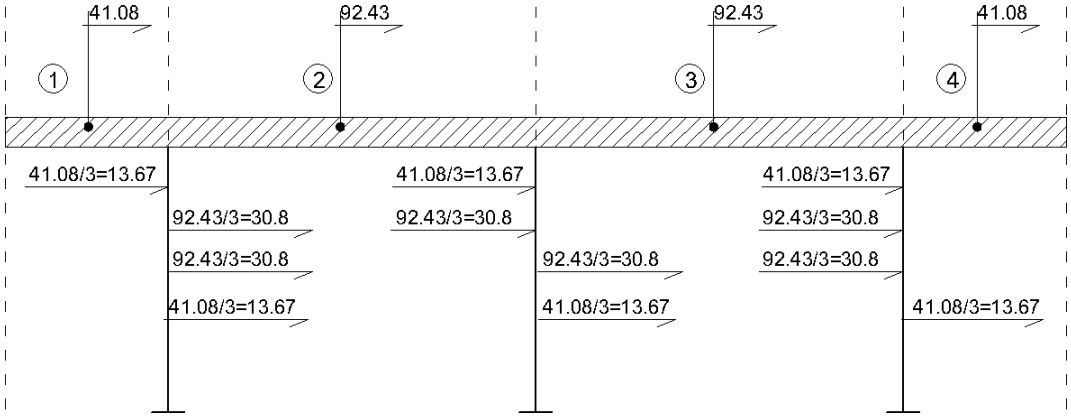

Figure 2.P

Total axial force diagram

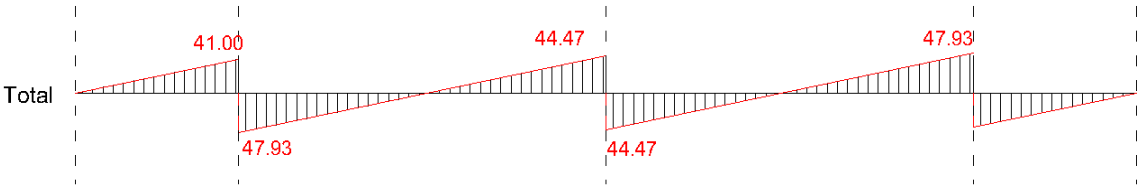

Figure 2.R and Figure 2.S shows the manual drawings for the shear force and bending moment diagrams:

Figure 2.Q

Free body diagram

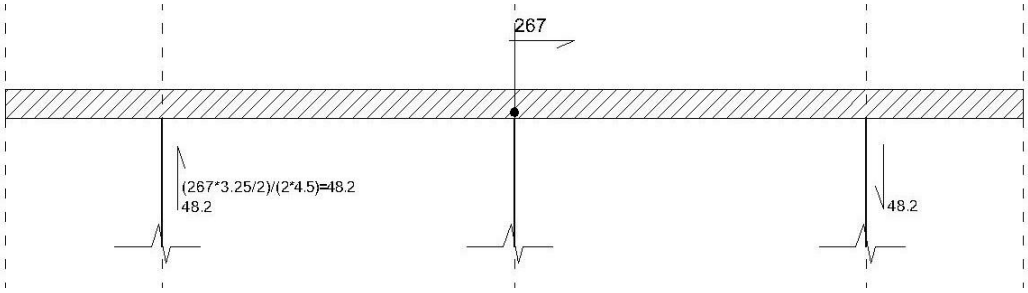

Figure 2.R

Shear force diagram-manual

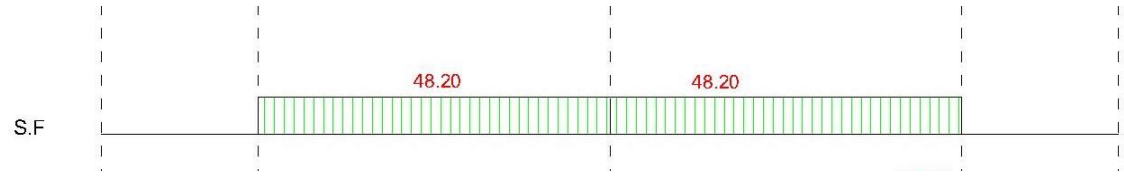

Figure 2.S

Bending moment diagram-manual

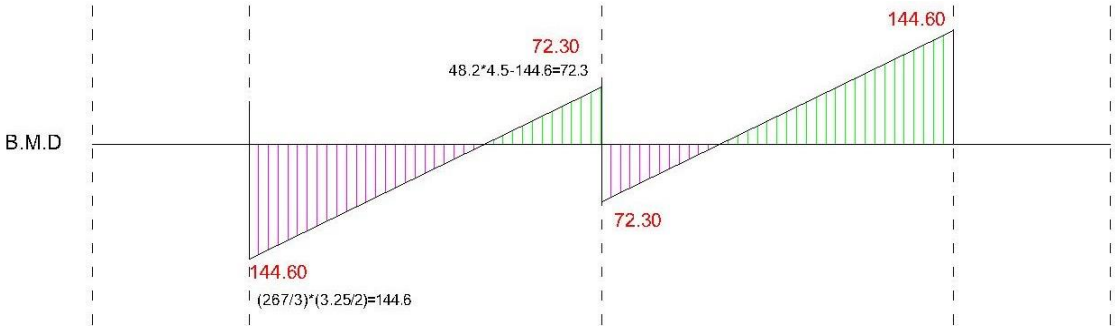

The forces and stresses due to horizontal earthquake component in Y direction with eccentricity of 1 meter can't be figured manually.

The forces and stresses due to vertical earthquake component in Z direction are shown in Figure 2.T to Figure 2.T

Shear force developed per 1 meter run:

$$\mathrm{V} = \frac{(4.5 * 1) * (3 + 0.97 * 0.19 * 25)}{9.81} * (0.12 * 9.81) = 4.1\mathrm{kN}$$

Figure 2.T

Vertical component effect as a distributed load

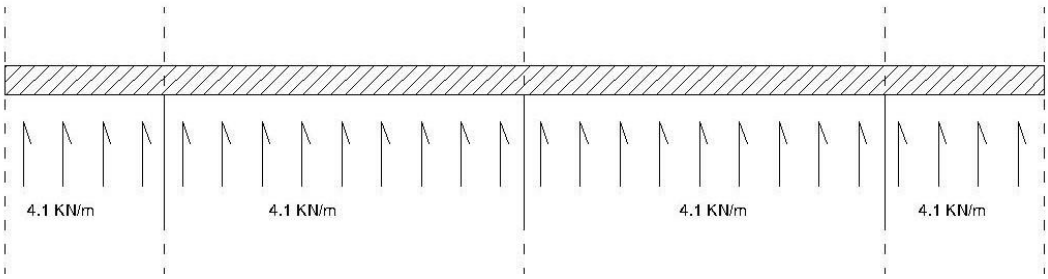

Figure 2.U

Manual shear force diagram due to vertical component.

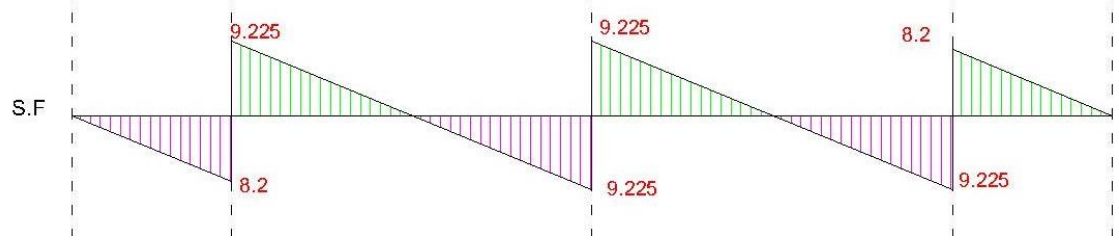

Figure 2.V

Manual bending moment diagram due to vertical component.

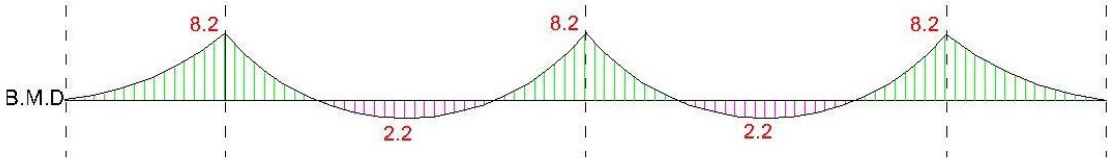

ETABS results

In this part ETABS results are listed to be compared with manual result, at the beginning Weight and Base Reaction Results are shown in Table 2.C:

Table 2.C

ETABS results for base reaction due to dead load and super imposed results.

Output Case	FZ(kN)
Dead	313.4137
S.I.D	175.5

When the modal analysis completed the mode shapes, natural periods, and natural frequencies can be extracted from ETABS as shown in Table 2.D:

Table 2.D

ETABS modal analysis result for the verification model

Mode	Period	UX	UY	UZ	RY	RZ	Frequency	CircFreq	Eigenvalue
	sec						cyc/sec	rad/sec	rad²/sec²
1	0.244	0	1	0	0	0	4.096	25.7375	662.4167
2	0.244	1	0	0	0.0018	0	4.101	25.7683	664.0075
3	0.225	0	0	0	0	1	4.447	27.9398	780.6349
4	0.023	0	0	0	0.998	0	43.7	274.576	75391.959
5	0.022	0	0	0.9997	0	0	44.596	280.2037	78514.1072

Table 2.E below shows ETABS resultant forces and stresses in columns and at structure base due to horizontal component in X direction:

Table 2.E

ETABS result for columns and structure base due to horizontal component in X direction

Sd	V_ Total	V_column	M_total	M_column	P_column
(m)	(kN)	(kN)	(kN.m)	(kN.m)	(kN)
0.00890	280.1762	46.61	916.2536	76.10	25.52

Table 2.F shows ETABS resultant forces and stresses in columns and at the structure base due to the horizontal component in the Y direction with an eccentricity of 1 m:

Table 2.F

ETABS result for columns and structure base due to horizontal component in Y direction with eccentricity of 1meter

Sd	Rϑ	V-Total	V-C2	V-C1,3	M-total	M-C2	M-C1,3	P-C2	P-C(1,3)
0.0089	0.00046	280.2	46.7	57.5	911.9	76.2	94	33.7	38.1

Table 2.G below shows ETABS resultant forces and stresses in columns and at the structure base due to the vertical component in the Z direction:

Table 2.G

ETABS result for columns and structure base due to vertical component in Z direction

Sd	P	P-total
$\mathbf{1.5 * 10^{-5}}$	56.022	336.13

Shell Stresses

In this part, the results of shell stresses don't agree with the results of manual calculations due to the load of the response spectrum, the main reason for this difference is the ETABS envelope method. When ETABS is a finite element software, the shell forces were calculated based on shell mesh elements, and the response spectrum results are presented as envelope results, which are significantly affected by the size of the shell mesh and the number of mesh elements and nodes, as shown in Appendix A.

The ETABS problem can be mathematically explained by the fact that when ETABS applying a two response spectrum load to simulate the earthquake action and display the envelope results, ETABS uses the formula $((\sum \text{max. of join force}))$, which depends on the number of joints and mesh size, while the manual calculation uses the formula $((\text{max. of } \sum \text{join force}))$.

To avoid this error, a static earthquake load equivalent to the load of the response spectrum was defined to read the forces and stresses of the shells in ETABS; this method will be used in the next chapters.

The forces and stresses in the slab due to the horizontal component in the X direction were plotted in ETABS using the Design Strip tool. Figure 2.W shows the axial force diagram, Figure 2.X the shear force diagram and Figure 2.Y the bending moment diagram:

Figure 2.W

ETABS Axial force diagram due to horizontal component in X direction

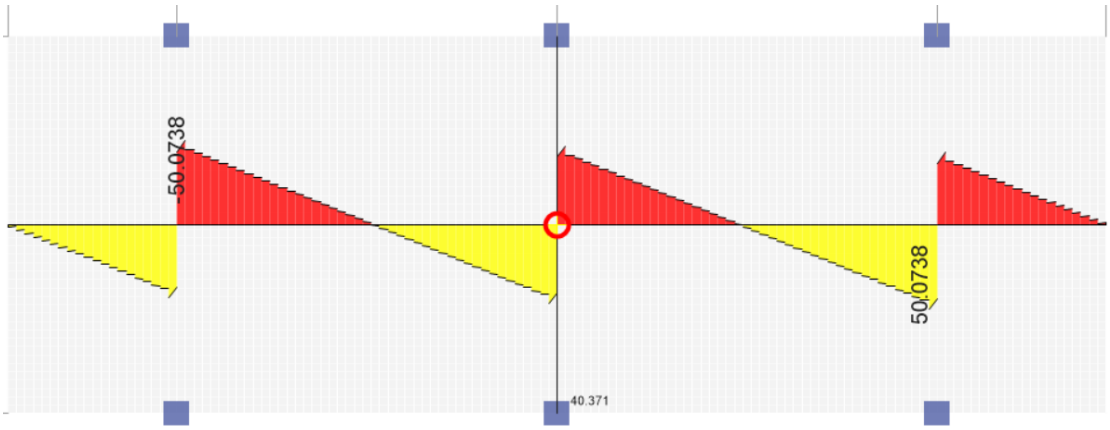

Figure 2.X

ETABS shear force diagram due to horizontal component in X direction

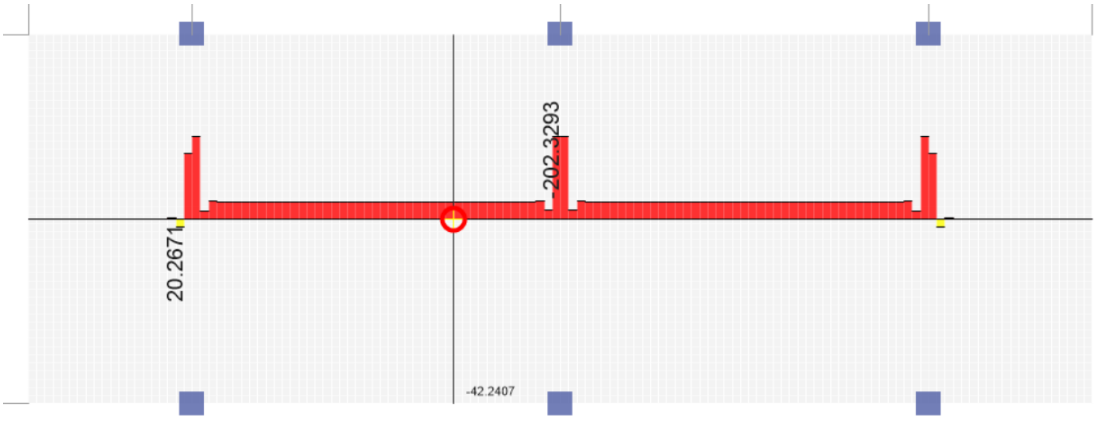

Figure 2.Y

ETABS bending moment diagram due to horizontal component in X direction

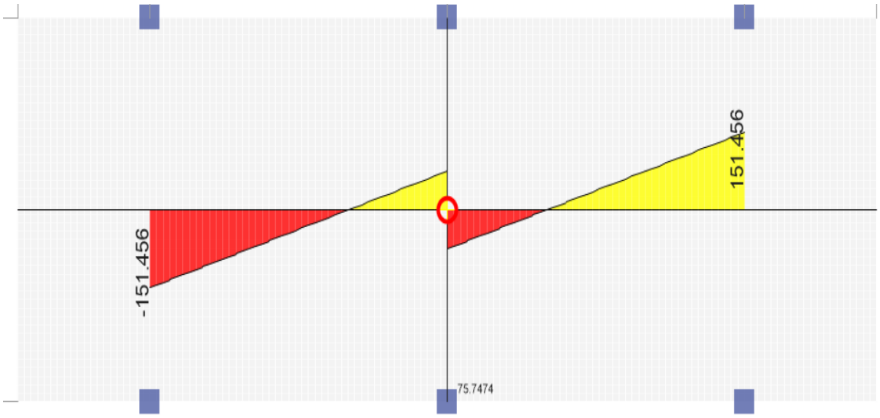

The forces and stresses in the slab due to the horizontal component in the y-direction with an eccentricity of 1 meter were neglected because they cannot be plotted manually. The forces and stresses in the slab due to the vertical component in the Z direction were plotted in ETABS using the Tool Design Strip. The results of the axial force are almost zero, Figure 2.Z shows the shear force diagram and Figure 2.AA the bending moment diagram:

Figure 2.Z

ETABS shear force diagram due to vertical component in Z direction

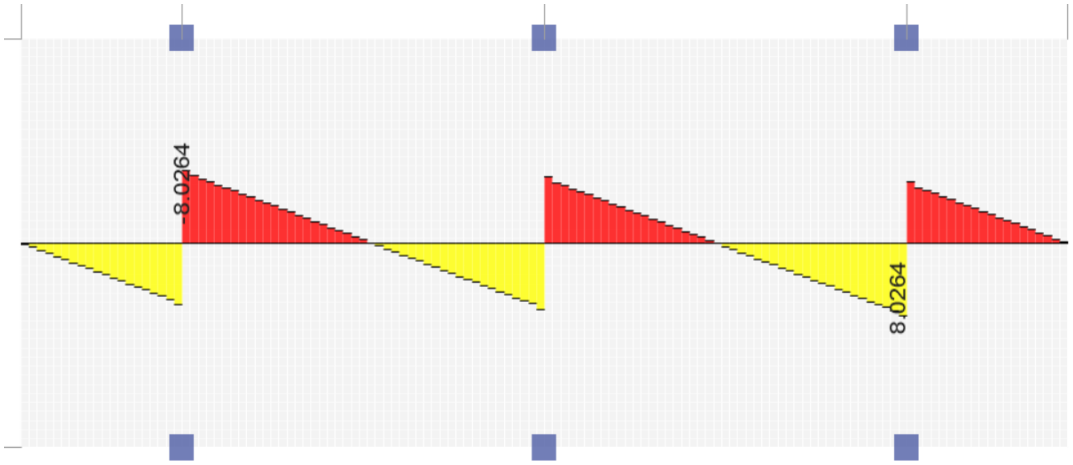

Figure 2.AA

ETABS bending moment diagram due to vertical component in Z direction

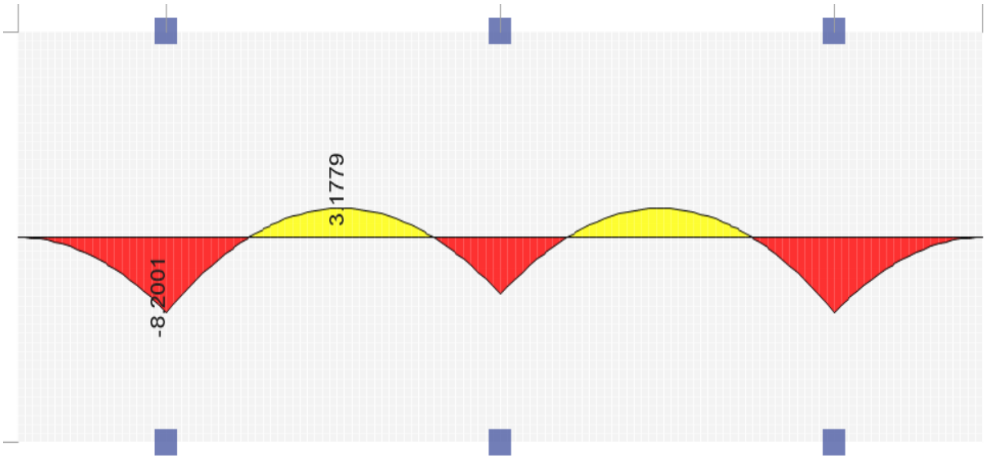

Percentages of difference between ETABS and manual results

Finally, to compare the ETABS result with the manual result, we need to calculate the percentage difference, as indicated in the ETABS verification manual. Table 2.H shows the list of manual calculation results, the ETABS results, and the percentage difference between the manual and ETABS results.

Table 2.H

Percentage of difference between the manual and ETABS results

		manual results	ETABS Results	%Difference
Modal analysis results.	mode 1(Ux) Period	0.246	0.244	-0.81%
	mode 2(Uy) Period	0.246	0.244	-0.81%
	mode 3(Rz) Period	0.226	0.225	-0.44%
	mode 5(Uz) Period	0.0227	0.022	-3.08%
	mode 1(Ux) frequency	25.57	25.7375	0.66%
	mode 2(Uy) frequency	25.57	25.7683	0.78%
	mode 3(Rz) frequency	27.75	27.9398	0.68%
	mode 5(Uz) frequency	277.055	280.2037	1.14%
Horizontal component in X direction results.	Sd	0.0086	0.0089	3.49%
	V-total	280.34	289.18	3.15%
	V-col	46.72	46.61	-0.24%
	M-total	911.1	916.25	0.57%
	M-col	75.92	76.1	0.24%
	P-col	25.3	25.52	0.87%
	Axial force in slab (max.)	47.93	50.07	4.46%
	Shear force in slab (max.)	48.2	42.24	-12.37%
	Bending moment in slab (max.)	144.6	151.46	4.74%
Horizontal component in Y direction with ecc. Of 1m results.	Sd	0.0086	0.0089	3.49%
	R9	0.00046	0.00046	0.00%
	V-total	280.34	280.18	-0.06%
	V-C2	46.73	46.7	-0.06%
	V-C1,3	58.05	57.5	-0.95%
	M-total	911.1	911.94	0.09%
	M-C2	75.94	76.19	0.33%
	M-C1,3	94.33	94	-0.35%
	P-C2	33.75	33.7	-0.15%
	P-C1,3	41.92	38.1	-9.11%
Vertical component in Z direction	Sd	0.000015	0.000015	0.00%
	P-col	56.17	56.022	-0.26%
	Axial force in slab (max.)	0	0	0.00%
	Shear force in slab (max.)	9.225	8.03	-12.95%
	Bending moment in slab (max.)	8.2	8.2	0.00%

Second verification model results

Another model with same properties, loaded with 18.5kN/m at cantilevers ends and analyzed in ETABS as shown in Figure 2.AB.

Figure 2.AB

3D view for the second verification model.

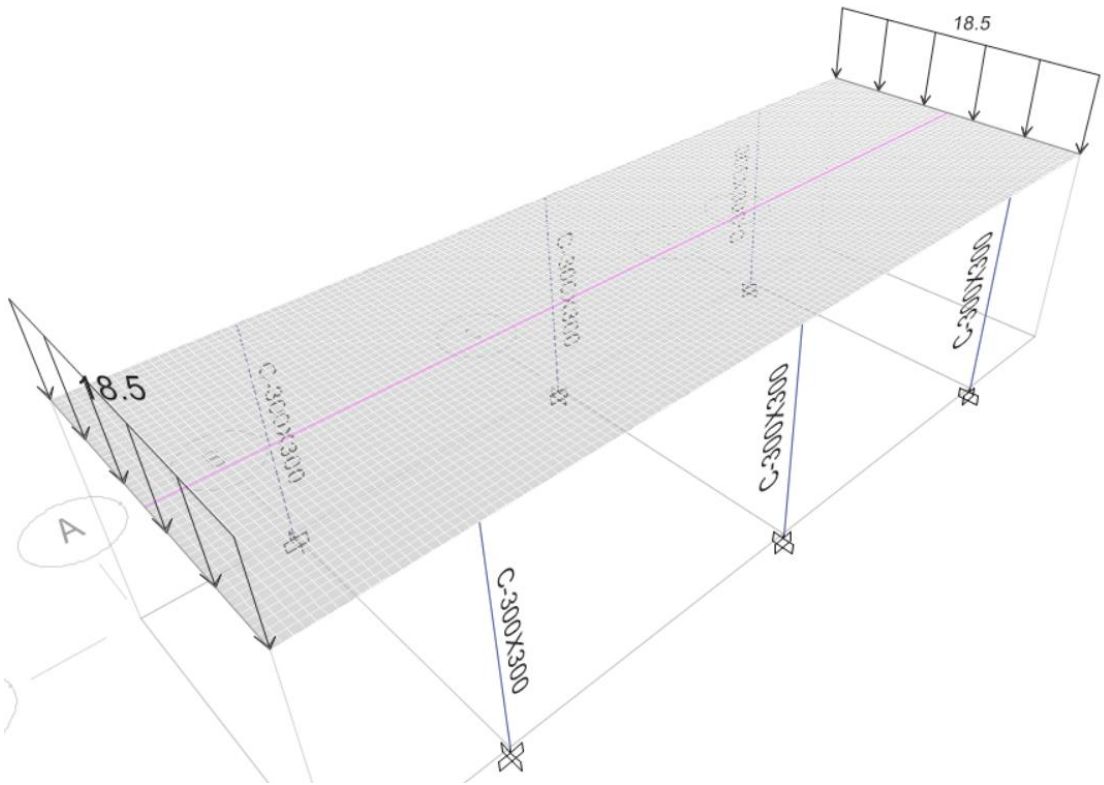

Analysis results were calculated manually to compute the difference percentage between ETABS results and manual as shown in Table 2.I:

Table 2.I

Percentage of difference between the manual and ETABS results

		manual results	ETABS Results	%Difference
Modal analysis results.	mode 1(Ux) Period	0.284	0.284	0.00%
	mode 2(Uy) Period	0.284	0.285	0.35%
	mode 3(Rz) Period	0.342	0.324	-5.26%
	mode 5(Uz) Period	0.0263	0.028	6.46%
	mode 1(Ux) frequency	22.089	22.11	0.10%
	mode 2(Uy) frequency	22.089	22.07	-0.09%
	mode 3(Rz) frequency	18.34	19.4	5.78%
	mode 5(Uz) frequency	239.29	227.8	-4.80%
Horizontal component in X direction results.	Sd	0.012	0.012	0.00%
	V-total	393.24	380.07	-3.35%
	V-col	65.54	63.35	-3.34%
	M-total	1278	1244.149	-2.65%
	M-col	106.5	103.05	-3.24%
	P-col	35.5	34.78	-2.03%
	Axial force in slab (max.)	90.95	94.44	3.84%
	Shear force in slab (max.)	66.25	61.11	-7.76%
	Bending moment in slab (max.)	198.74	205.49	3.40%
Horizontal component in Y direction with ecc. Of 1m results.	Sd	0.012	0.01203	0.25%
	R9	0.00065	0.000623	-4.15%
	V-total	391.17	380.0787	-3.35%
	V-C2	65.2	63.34	-3.36%
	V-C1,3	81	78.18	2.25%
	M-total	1271.3	1237.935	-3.14%
	M-C2	105.95	103.37	-2.94%
	M-C1,3	1313.625	127.27	2.43%
	P-C2	47.09	45.85	-3.14%
	P-C1,3	55.22	47.6	-13.80%
Vertical component in Z direction results.	Sd	0.000021	0.000021	0.00%
	P-col	73.02	72.8	-0.3%
	Axial force in slab (max.)	0	0	0.00%
	Shear force in slab (max.)	18.19	16.64	-8.52%
	Bending moment in slab (max.)	29.6	30.1	1.69%

The large difference in shear force in the slab refer to the stress concentration in the column region which is not visible in the manual calculations.

Based on the previous results, the ETABS result is almost accepted, the ETABS software can be adopted.

2.5 Study sections

Effect of cantilever directions on the structure seismicity

Each of the first set structures was modeled and analyzed in the ETABS software without including accidental torsion effect. The periods of the models, the sequence of modes, and the diaphragms drift were extracted from the ETABS models. The results were listed in tables and compared to understand how the directions and positions of the cantilevers affect the response of the structures and the nature of the vibration modes.

Effect of Cantilever Length and Load on the sequence of Modes

The effect of cantilever length and concentrated load at the end on the sequence of vibration modes is investigated by constructing 16 models as explained in the second set of models, where each four models represent a specific architectural style and the concentrated load at the ends of the cantilevers was selected according to their architectural style.

The first group simulates a cantilever with light curtain walls, and the equivalent load for the curtain walls was set to zero.

The second group simulates a balcony with a parapet of 1 m height, where the equivalent load for the parapet walls was chosen to be 6 kN/m.

The third group of models simulates a cantilevered room with a window, where the equivalent load for the wall with window opening was chosen to be 12 kN/m.

The fourth group of models simulating a cantilevered room with a closed wall, where the equivalent load for the solid walls was chosen to be 18 kN/m.

Each of the aforementioned groups contains four models with different cantilever lengths, where the cantilever lengths were selected based on the most commonly used cantilevers (0.5 m, 1 m, 1.5 m, 2 m).

Upon completion of the dynamic analysis, the results of the natural period, and mode shapes (extracted for each model), as well as plots of period versus cantilever length (Lc/Ls), are produced for each set of cantilever patterns.

Effect of cantilever length and load on shear capacity

The effect of cantilever length and concentrated load at its end on shear capacity is investigated. Using the model sets previously defined, the shear capacities of slabs and beams are calculated based on Equation (5.1) in S.I. units as specified by the American Concrete Institute in Building Code Requirements for Structural Concrete and Commentary (ACI 318-14).

$$V_c = 0.17\lambda\sqrt{f'_c}b_w d \qquad (2.21)$$

Where λ is modification factor related to concrete unit weight and equal 1 for normal weight concrete and bw is the section width and d is the effective depth of the section. The horizontal earthquake component was imposed to the structures and their effect on beams and slabs was examined using ETABS model. When axial tension forces were taken in account, the shear capacity shall be reduced as indicated in Equation (2.22) based on ACI 318-14

$$V_c = 0.17\left(1 + \frac{N_u}{3.5Ag}\right)\lambda\sqrt{f'_c}b_w d \qquad (2.22)$$

Where Nu is the axial force in kN and negative for tension.

Site effects on the behavior of loaded and unloaded cantilevers under earthquake components in different directions.

A four-story reinforced concrete structure with a ribbed slab system of 25 cm and hidden beams 60 cm wide and 25 cm deep for the main beams and square columns of 30 cm was modeled and analyzed in ETABS. The structure was analyzed four times with different horizontal and vertical earthquake components. The earthquake spectral

acceleration, the earthquake spectral response parameters at short periods (SDS) and the earthquake spectral response parameters at a period of 1s (SD1) were selected to represent four Palestinian cities (Jericho, Nablus, Hebron, beer Saba), and the response spectrum curves represent one of these four cities respectively.

Figure 2.AC below shows the seismic zone map for Palestinian cities.

Figure 2.AC

Seismic zone map for Palestine

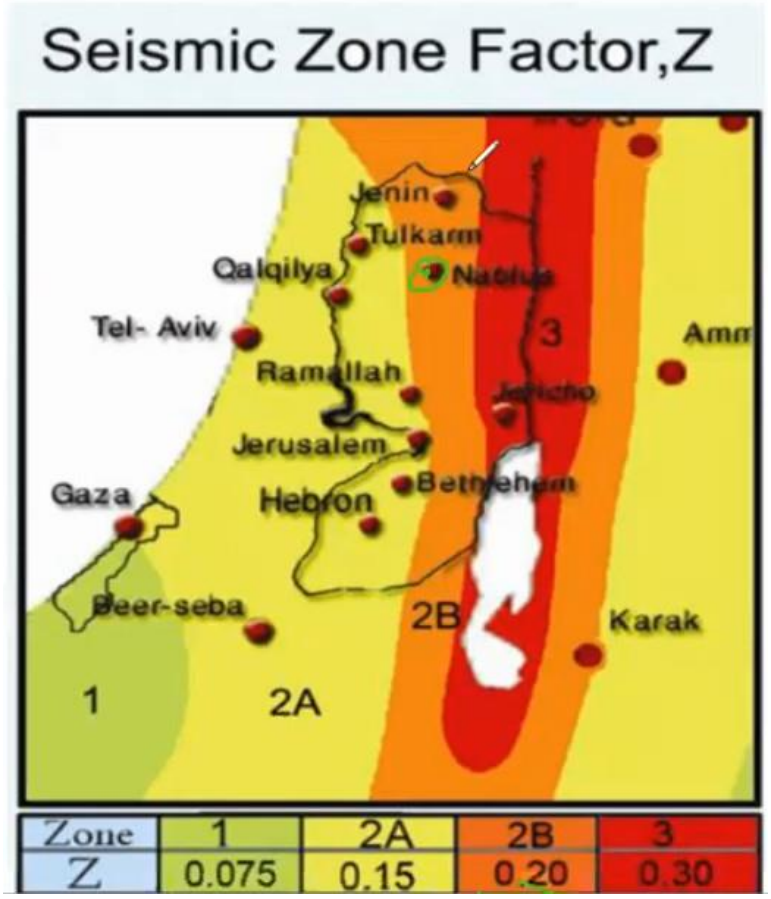

The results of axial force, shear force and bending moment were recorded at the start point of the cantilever (connection between cantilever and column), and the analysis was repeated one more time considering the additional masonry load at the end of the cantilever. The purpose of the second analysis is to determine the ratio of the increase in seismic forces due to the masonry load in each city.

Chapter Three

Results

3.1 Effect of cantilever directions on the structure seismicity

The analysis results were divided into three parts, starting with the sequence of modes and the effect of cantilevers on torsional modes, the availability of inherent torsion, diaphragm displacement, and the level of torsional irregularity (no torsional irregularity, torsional irregularity, or extreme torsional irregularity).

Sequence of modes

In the first model, single side cantilever model was studied and analyzed. Table 3.1 shows the first three modes periods and the modal participation mass ratios:

Table 3.A

Single side model, periods and modal participation mass ratios results.

Case	Mode	Period	UX	UY	RZ
Modal	1	0.336	0	0.8791	0.1239
Modal	2	0.327	0.9945	0	0
Modal	3	0.264	0	0.12	0.8729

The structure was horizontally irregular and had an eccentricity of 1 m in the X direction. The first mode was mainly translation and coupled with torsion mode, the second mode was completely translation and the third mode was torsion and coupled with translation.

In the second model, a double side in the same direction cantilever model was investigated and analyzed. Table 3.2 shows the first three modes, the periods and the modal participation mass ratios.

Table 3.B

Double side in same direction model, periods and modal participation mass ratios results.

Case	Mode	Period	UX	UY	RZ
Modal	1	0.353	0.9916	0	0
Modal	2	0.346	0	0.9992	0
Modal	3	0.318	0	0	0.9957

The structure was horizontally regular and had no eccentricities. The first and second modes were translational modes and the third mode was a torsional mode.

In the third model, double side in different directions cantilever model has been studied and analyzed, Table 3.3 shows the periods of the first three modes and modal participation mass ratios.

Table 3.C

Double side in different directions model, periods and modal participation mass ratios results.

Case	Mode	Period	UX	UY	RZ
Modal	1	0.383	0.3791	0.3791	0.2455
Modal	2	0.355	0.4976	0.4976	0
Modal	3	0.296	0.1189	0.1189	0.7506

The structure was horizontally irregular and had an eccentricity of 1 m in the X and Y directions. The first mode was a coupled mode of translation in both directions and torsion mode, the second mode was a coupled mode of translation in both directions, and the third mode was mainly torsion and coupled with translation.

In the fourth model, triple side cantilevers model has been studied and analyzed, Table 3.4 shows the periods of the first three modes and the modal participation mass ratios.

Table 3.D

Triple side model, periods and modal participation mass ratios results.

Case	Mode	Period	UX	UY	RZ
Modal	1	0.407	0	0.6646	0.3356
Modal	2	0.38	0.9965	0	0
Modal	3	0.346	0	0.3288	0.6609

The structure was horizontally irregular and had an eccentricity of 1 m in the Y direction. The first and third vibration modes were coupled translational and torsional vibrations, and the second vibration mode was a translational vibration.

In the fifth model, Fourfold side cantilever model was studied and analyzed, Table 3.5 shows the first three modes period and modal participation mass ratio.

Table 3.E

Fourfold side model, periods and modal participation mass ratio results.

Case	Mode	Period	UX	UY	RZ
Modal	1	0.42	0	0	0.9978
Modal	2	0.41	0.0006	0.9941	0
Modal	3	0.41	0.9941	0.0006	0

The structure was horizontally regular and have no eccentricities. The first modes was torsional mode, and the second and third modes were translation modes.

Inherent torsion analysis

According to the previous results, the inherent torsion is clearly present in the irregular structures (models with single cantilever, double cantilever in different directions and triple cantilever), which can lead to additional torsional response, but in the regular models (models with double cantilever in the same direction and Fourfold cantilever models), the effect of inherent torsion is neglected, which can improve the response of the structure.

Regular models will be used in the next chapters, and irregular models will be avoided to be discussed in later researches.

Torsional irregularity

The torsional irregularity index describes the level of sensitivity of the structure to the torsional effect due to earthquake action. The ASCE code classifies torsional irregularity based on the ratio of maximum story drift to average story drift and states that the structure has torsional irregularity if this ratio is greater than 1.2, and that the structure has extreme torsional irregularity if the ratio is greater than 1.4.and each one of these classes needs special design requirements and amplification of earthquake forces to be included in seismic design explained in the design code.

Table 3.F shows the maximum drift to average story drift for previously analyzed models:

Table 3.F

Maximum drift to average drift ratio.

model	max drift	Avg drift	max drift/Avg drift
Single side cantilever	0.000037	0.000026	1.412
Double sides in similar directions cantilever	0.000026	0.000026	1
Double sides in different directions cantilever	0.000027	0.000014	1.901
triple sides cantilever	0.000031	0.000018	1.719
Fourfold sides cantilever	0.000019	0.000019	1

As shown in the table above, the models with one single direction, double sides in different directions, and triple directions are models classified as extremely irregular torsional structures based on the ASCE code, requiring additional force amplification in seismic design.

3.2 Effect of Cantilever Length and Load on the sequence of Modes

The results of the dynamic analysis for the four groups of models, which include four models with cantilever lengths of (o.5 m, 1 m, 1.5 m, 2 m) and equivalent cantilever length to successive span length (Lc/Ls) of (11%, 22%, 33%, 44%), were analyzed and plotted on a graph to show the effect of cantilever length and loading on the sequence of vibration modes. Figure A.3 shows the results of the four model series, which is on the diagram the basic mode expected to torsional mode after 50% cantilever length to span length ratio (Lc/Ls) for the first series, which included cantilevers with curtain wall, this ratio isn't studied in this research and can read it from line extension because the relationships are approximately linear.

The fundamental mode expected to be torsional mode after 40% cantilever length to span length ratio (Lc/Ls) for the second set, the end of cantilever load selected to be 6kN/m to simulate the parapet wall pattern.

The fundamental mode expected to be torsional mode after 30% cantilever length to span length ratio (Lc/Ls) for the third set which is contain cantilevers loaded with 12kN/m to simulate the walls contain windows openings pattern. And the fundamental mode expected to be torsional mode after 22% cantilever length to span length ratio (Lc/Ls) for the fourth set, which contains cantilevers loaded with 18kN/m to simulate the solid walls pattern.

Figure 3.A

Cantilever load and length Effect on sequence of modes.

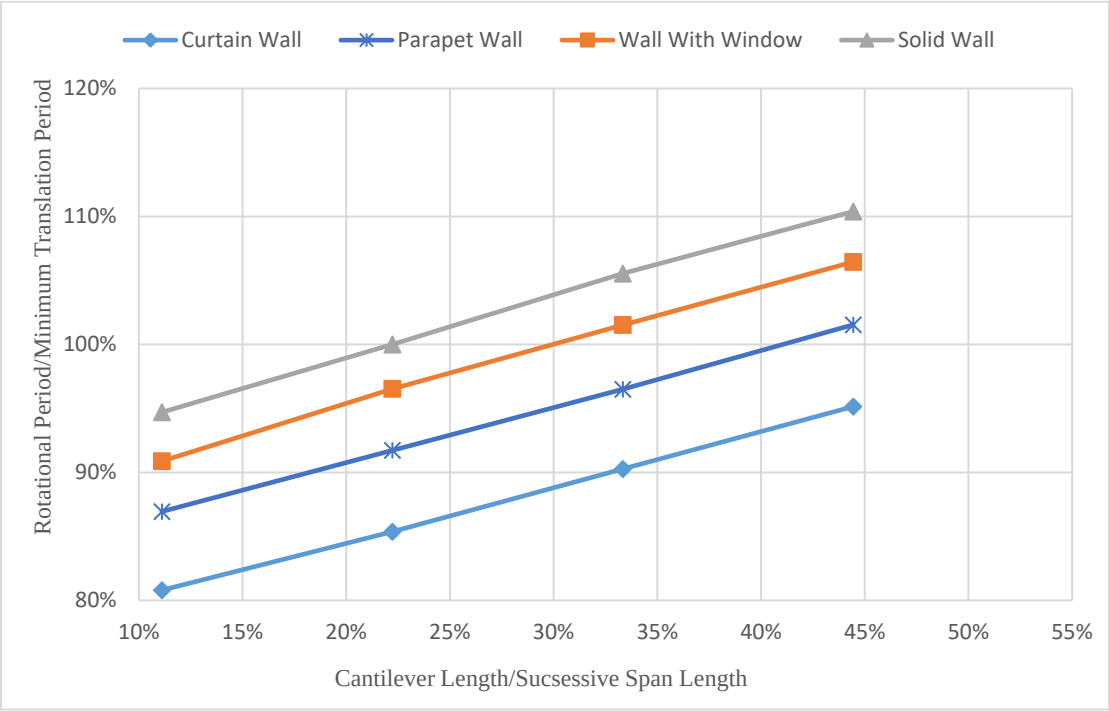

3.3 Effect of cantilever length and load on shear capacity

ETABS and code equations results for axial forces due to horizontal earthquake component and their effect on shear capacity in first story are listed in Table 3.G for cantilever beam and Table 3.H for cantilever slab.

Table 3.G

Effect of axial load on shear capacity in cantilever beam

	Cantilever Beam				
Set	**cantilever length**	**Vc**	**Axial Load**	**Vc with tension**	**%losses in shear capacity**
Curtain wall	0.5	73.29	3.95	73.08	0.28%
	1	73.29	7.52	72.90	0.54%
	1.5	73.29	11	72.71	0.79%
	2	73.29	14.1	72.55	1.01%
parapet wall	0.5	73.29	10.36	72.75	0.74%
	1	73.29	13.2	72.60	0.94%
	1.5	73.29	16	72.45	1.14%
	2	73.29	18.7	72.31	1.34%
Wall with window	0.5	73.29	16.8	72.41	1.20%
	1	73.29	18.8	72.30	1.34%
	1.5	73.29	21.1	72.18	1.51%
	2	73.29	23.3	72.07	1.66%
solid wall	0.5	73.29	23.19	72.07	1.66%
	1	73.29	24.44	72.01	1.75%
	1.5	73.29	26.13	71.92	1.87%
	2	73.29	27.9	71.83	1.99%

Table 3.H

Effect of axial load on shear capacity in cantilever slab

Cantilever slab (results for each rib)					
Set	**cantilever length**	**Vc**	**Axial Load**	**Vc with tension**	**%losses in shear capacity**
curtain wall	0.5	21.99	0.34	21.97	0.08%
	1	21.99	0.73	21.95	0.17%
	1.5	21.99	1.15	21.93	0.27%
	2	21.99	1.66	21.90	0.40%
parapet wall	0.5	21.99	0.75	21.95	0.18%
	1	21.99	1.30	21.92	0.31%
	1.5	21.99	1.85	21.89	0.44%
	2	21.99	2.46	21.86	0.59%
Wall with window	0.5	21.99	1.15	21.93	0.27%
	1	21.99	1.88	21.89	0.45%
	1.5	21.99	2.55	21.85	0.61%
	2	21.99	3.26	21.82	0.78%
solid wall	0.5	21.99	1.57	21.90	0.37%
	1	21.99	2.45	21.86	0.58%
	1.5	21.99	3.26	21.82	0.78%
	2	21.99	4.06	21.77	0.97%

3.4 Site effects on the behavior of loaded and unloaded cantilevers under earthquake components in different directions

After the analysis was performed and checked, the forces and stresses due to the horizontal and vertical earthquake components were extracted and listed in tables to compare them. Table 3.I and Table 3.J show the analysis results for the first story.

Table 3.I

Forces and stresses due to horizontal earthquake component for the first story

	horizontal Earthquake component					
	without masonry wall load effect			**With masonry wall load effect**		
City	**Axial force**	**Shear force**	**Bending moment**	**Axial force**	**Shear force**	**Bending moment**
Jericho	16.3	163.3	80.4	27.3	178.6	88
Nablus	10.8	108.7	53.5	18.8	122.7	60.4
Hebron	8.3	83.6	41.1	14.4	94.4	46.5
Beer Saba	4.9	48.8	24	8.5	55.34	27.24

Table 3.J

Forces and stresses due to vertical earthquake component for the first story

	vertical earthquake component					
	without masonry wall load effect			**With masonry wall load effect**		
City	**Axial force**	**Shear force**	**Bending moment**	**Axial force**	**Shear force**	**Bending moment**
Jericho	0	5	4.33	0	10.85	11.8
Nablus	0	3.8	3.3	0	8.3	9
Hebron	0	3.2	2.8	0	7	7.6
Beer Saba	0	1.86	1.63	0	4.1	4.43

From the above tables it is clear that the horizontal component of the earthquake has a greater effect than the vertical one, causing greater forces and stresses. The reason is that the vertical component of the earthquake is a ratio of horizontal component, and the vertical component acts vertically on the structures and causes mainly axial forces that the supporting elements of the structure can easily resist, and it is known that reinforced concrete structures have a large capacity to resist axial forces. On the other hand, the horizontal earthquake component acts on the structures in the form of bending forces and causes large deformations of the structural elements and cantilevers.

To determine the increasing ratio of seismic forces due to masonry loading, DA, Dv and DM are symbols that represent the change of forces of structural elements due to the change of masonry loading as explained in equations (6.1), (6.2) and (6.3).

$$D_A = \frac{\text{axial force with masonry wall effect} - \text{axial force without masonry wall effect}}{\text{masonry wall load}} \quad (3.1)$$

$$D_V = \frac{\text{shear force with masonry wall effect} - \text{shear force without masonry wall effect}}{\text{masonry wall load}} \quad (3.2)$$

$$D_M = \frac{\text{bending moment with masonry wall effect} - \text{bending moment without masonry wall effect}}{\text{masonry wall load}} \quad (3.3)$$

Equations results due to vertical and horizontal earthquakes components were plotted in terms of base rock acceleration (Z),Figure 3.B,Figure 3.C, and Figure 3.D shows the change in axial force, shear force, and bending moment, respectively. Each diagram contains two curves, one showing the results due to the horizontal earthquake component and the other showing the results due to the vertical earthquake component, as described in the figures.

Figure 3.B

Increase in axial force due to masonry wall load effect

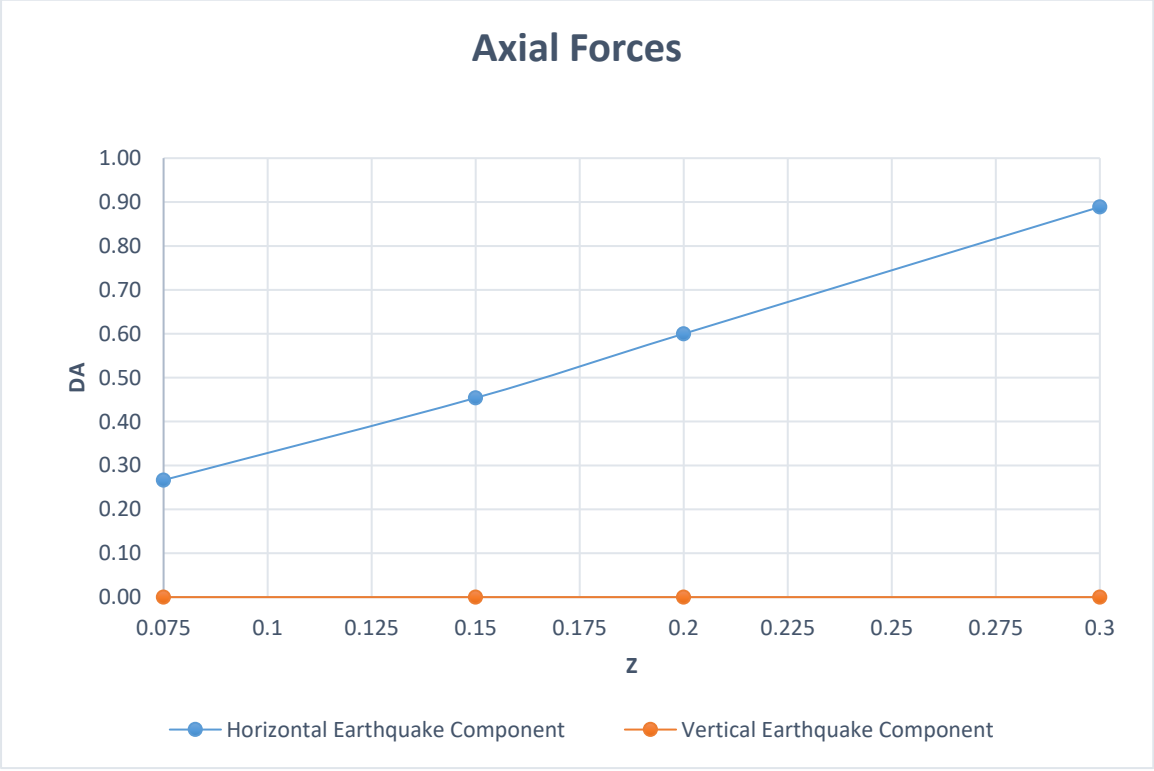

Figure 3.C

Increase in shear force due to masonry wall load effect

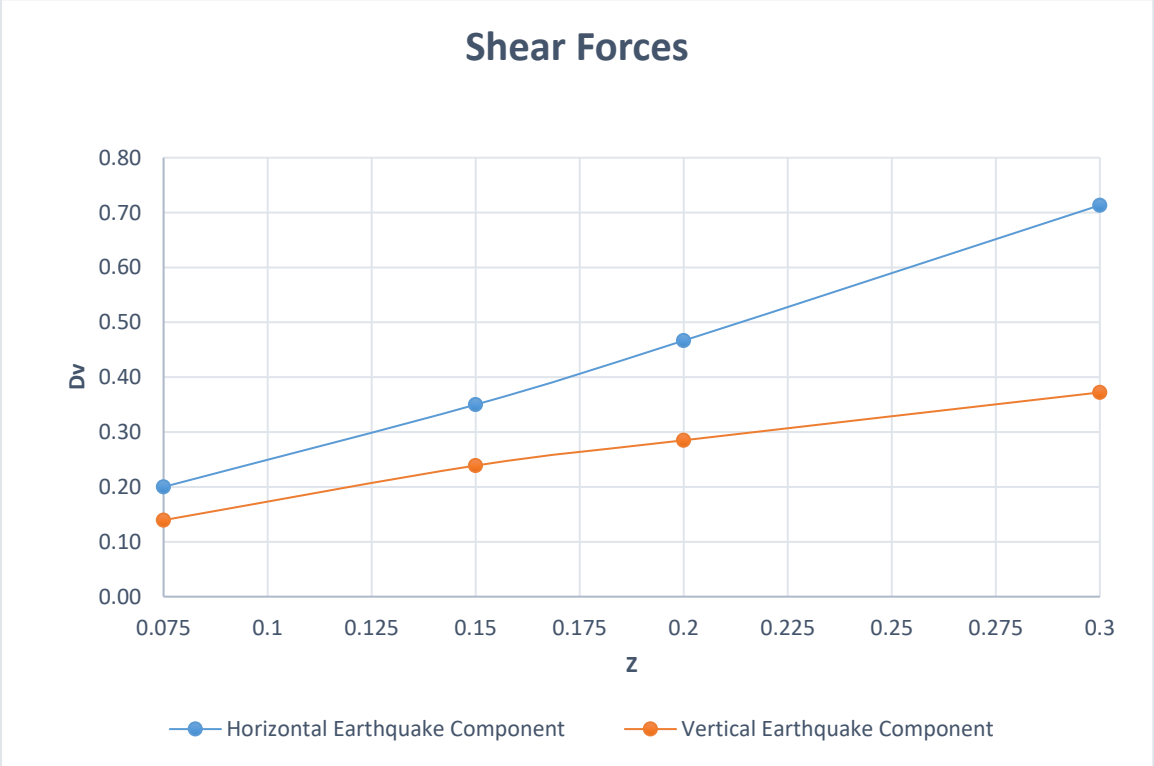

Figure 3.D

Increase in bending moment due to masonry wall load effect

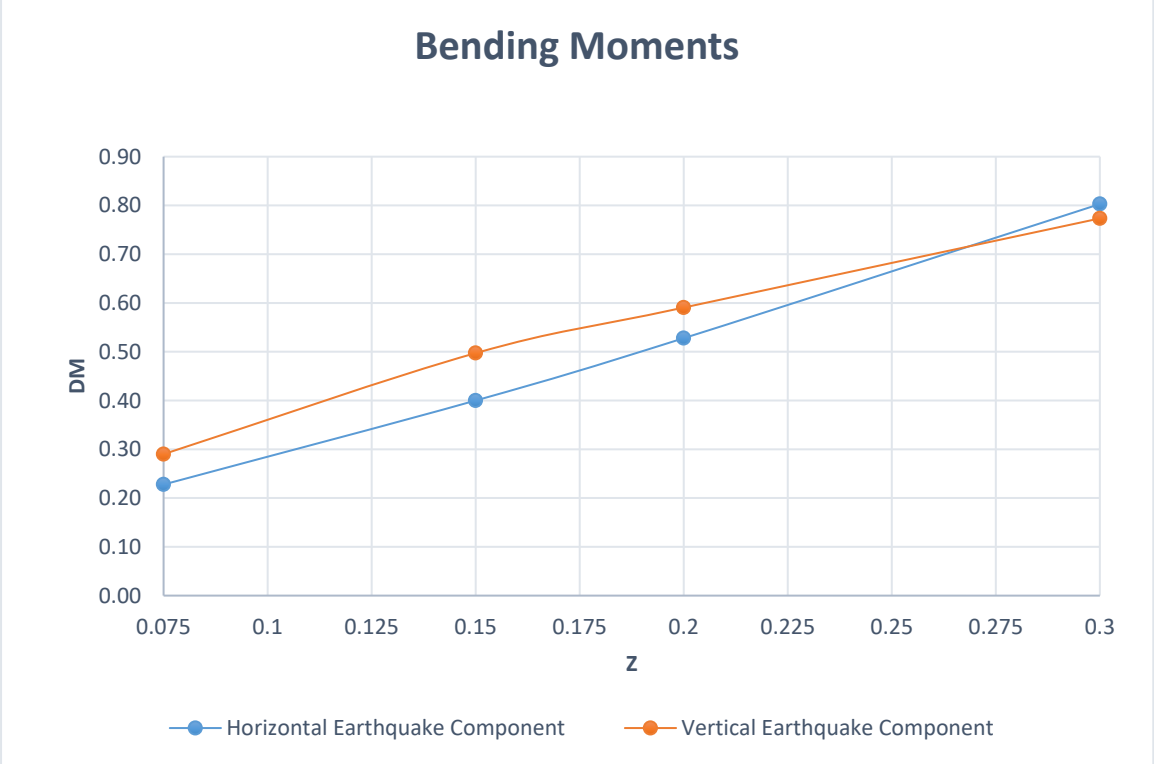

The curves in the previous graphs are not perfectly linear and do not increase at a constant rate between the different cities, which is related to the change in the curves of the response spectrum, as shown in Figure 3.E

Figure 3.E

Response spectrum curves for each city

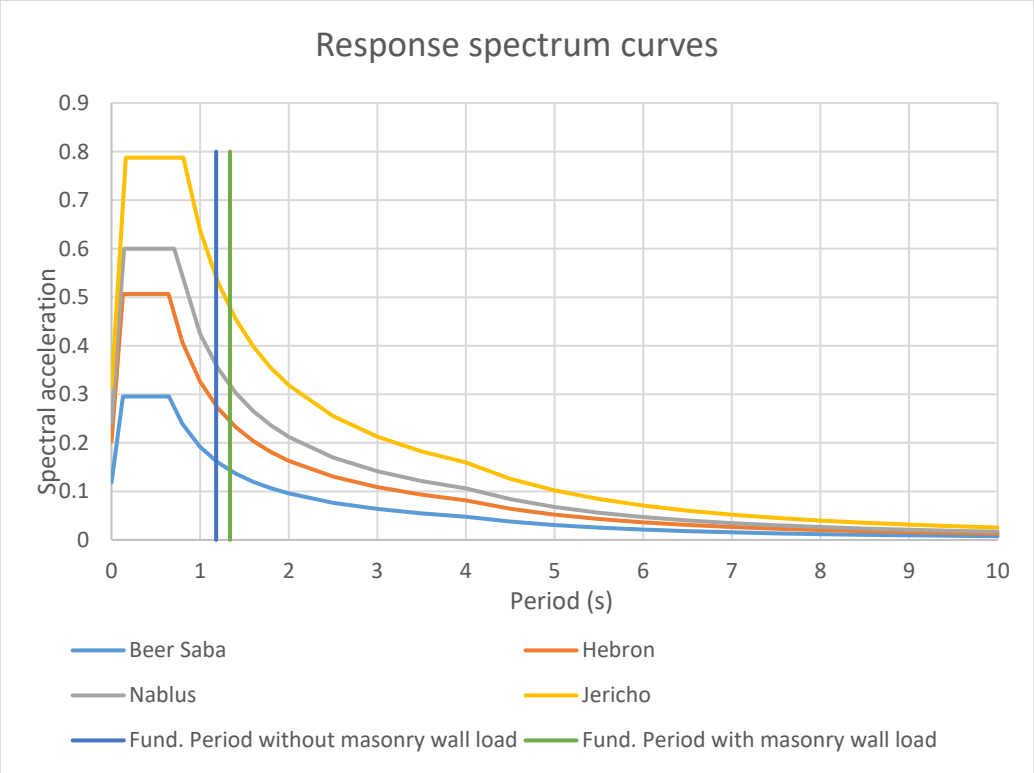

The next equation used to read the percent of increasing in stresses before masonry wall load added.

$$Percent\ of\ stresses\ increasing = \frac{stress\ result\ with\ masonty\ wall\ load - stress\ result\ without\ masonty\ wall\ load}{masonry\ wall\ load}\%$$

And Table 3.K shows the percent of increasing in stresses after adding masonry wall load due to vertical and horizontal component in each city

Table 3.K

The percent of increasing in stresses after adding masonry wall load

city	Horizontal component			Vertical component		
	Axial force	**Shear force**	**Bending moment**	**Axial force**	**Shear force**	**Bending moment**
Jericho	59%	83%	41%	0%	32%	40%
Nablus	43%	76%	37%	0%	24%	31%
Hebron	33%	58%	29%	0%	21%	26%
Beer Saba	19%	35%	18%	0%	12%	15%

Chapter Four
Discussions and Conclusions

- regular cantilever structure is a special case of regular structures don't have a torsional irregularity, but can induce a large torsional behavior, the Table 4.A shows the common forms of cantilever directions and distribution and their effect on the structure response.

Table 4.A

The common forms of cantilever directions and distribution and their effect on the structure response.

Model	regularity	1st mode direction	2nd mode direction	3rd mode direction
1-Single side cantilever	irregular	coupled Uy and Rz	Ux	coupled Rz and Uy
2-Double side cantilever in same direction	regular	Ux	Uy	Rz
3-Double side cantilever in different directions	irregular	coupled Uy, Ux, and Rz	coupled Uy and Ux	coupled Rz and(Ux, Uy)
4-Triple side cantilever	irregular	coupled Uy, and Rz	Ux	coupled Rz, and Uy
5-Fourfold cantilever	regular	Rz	Uy	Ux

As shown in the previous table, the models with irregular cantilever distribution (such as the first, third, and fourth models) produce coupled fundamental modes and usually involve torsional behavior, but the regular models (such as the second and fifth models) produce uncoupled fundamental modes and, in some cases, perhaps a pure torsional mode, because as the ratio of cantilever mass to total mass of the structure increases, the torsional behavior of the structure increases and the probability of obtaining a fundamental torsional mode increases.

- The presence of regular and opposite cantilevers minimizes the likelihood that an earlier torsional mode will occur.
- The sequence of modes was influenced by cantilever length. As the cantilever length increases, the fundamental period increases and the probability that the torsional modes occur before the translational modes increases.

Table 4.B

The critical percentage of the cantilever length in relation to the successive span length

Loading Case	Critical (Lc/Ls) Ratio
Curtain Wall (0kN)	~50%
Parapet Wall (6kN)	41%
Window Wall (12kN)	30%
solid Wall (18kN)	22%

- the results of the forces and stresses in the presence of masonry have an increase of 152% for axial forces and 13.4% for shear forces and bending moments due to the horizontal component of the earthquake, and an increase of 79% for shear forces and 157% for bending moments due to the vertical component of the earthquake, The difference in the increasing ratio relate to the method of how the

stresses were generated, the stresses in cantilevers due to horizontal component were generated due to lateral forces and due to large deformation in structural elements, but the stresses due to vertical component were generated due to axial loads in vertical elements (columns) and shear loads in horizontal elements (beams and slabs).

- The results show that the vertical earthquake component does not have an axial effect on the cantilevered sections because the forces due to the vertical component are transmitted through the load-bearing elements.
- The rate of stress increase is different in each city because the response spectrum curve does not have the same slope in different cities.
- The effect of axial stress due to the horizontal earthquake component on the shear capacity of sections can be neglected if the percentage loss of shear capacity does not exceed 2% for beams and 1% for ribs.
- The vertical earthquake component is not significant for the following reasons:
  - The stresses due to the vertical component act as axial loads in the vertical elements (columns) and as shear loads in the horizontal elements (beams and slabs).
  - The vertical earthquake component has no axial effect on the cantilevered sections because the induced forces due to the vertical component were transmitted through the load-bearing elements.
  - The horizontal component acts on the structure as a lateral load and causes large deformations and rotations in the connections.

Recommendations for later studies

- Repeat the study for irregular structures with coupled modes.
- Repeat the study for vertical earthquake component and apply it as detailed and independent response spectrum curve.
- Include bracing effect from nonstructural members.

List of Abbreviations

Abbreviation	Meaning
D	Dead load
e	Eccentricity
E_c	Concrete modulus of elasticity
f'_c	Concrete compressive strength
K_c	The column stiffness
k_u	The translational stiffness coefficient in x direction.
k_v	The translational stiffness coefficient in y direction.
K_{yi}	Y-direction stiffness of i frame
K_z	The axial stiffness coefficient.
k_ϑ	The rotational stiffness coefficient about z axis.
M	Bending moment
m_v	The translational mass coefficients in y direction
m_z	The vertical translation mass coefficient and
m_ϑ	Mass polar moment of inertia
P	Axial force
Sa	Pseudo acceleration.
Sd	Story drift.
SID	Superimposed dead
T_u	Natural period for first flexural mode.
T_v	Natural period for second flexural mode.
T_z	Natural period for axial mode.
T_ϑ	Natural period for torsional mode.
m_u	The translational mass coefficients in x direction
V	Shear force
V_{yi}	Shear force in y-direction in i frame
X_i	Distance from frame i to center of gravity of the floor in x-direction
y_i	Distance from frame i to center of gravity of the floor in y-direction
Υ_c	Concrete unit weight
ω_u	Natural frequency for first flexural mode.
ω_v	Natural frequency for second flexural mode.
ω_z	Natural period for axial mode.
ω_ϑ	Natural frequency for torsional mode.

References

[1] Yurdakul, Ö., Duran, B., Tunaboyu, O., & Avşar, Ö. (2020). Field reconnaissance on seismic performance of RC buildings after the January 24, 2020 Elazığ-Sivrice earthquake. *Natural Hazards*, *105*(1).

[2] KORKMAZ, H. H. (2018). Overhangs in structural systems and earthquake behaviour from torsional irregularity point of view. *Selcuk University Journal of Engineering, Science and Technology*, *6*(3).

[3] Minimum Design Loads and Associated Criteria for Buildings and Other Structures. 2017;

[4] Tesfamariam, S., Goda, K., & Mondal, G. (2015). Seismic vulnerability of reinforced concrete frame with unreinforced masonry infill due to main shock–aftershock earthquake sequences. *Earthquake Spectra*.

[5] Armouti NS. Earthquake engineering: Theory and implementation with the 2015 International Building Code. New York etc.: McGraw-Hill Education; 2015.

[6] Chopra. Dynamics of Structures: Theory and applications to earthquake engineering. Boston etc.: Pearson; 2015.

[7] 318-14: Building code requirements for structural concrete and commentary. 2014;

[8] Mondal, G., & Tesfamariam, S. (2013). Effects of vertical irregularity and thickness of unreinforced masonry infill on the robustness of RC framed buildings. *Earthquake Engineering & Structural Dynamics*.

[9] Mondal G, Tesfamariam S. Effects of vertical irregularity and thickness of unreinforced masonry infill on the robustness of RC framed buildings. Earthquake Engineering & Structural Dynamics. 2013.

[10] Inel M, Ozmen HB, Bilgin H. Re-evaluation of building damage during recent earthquakes in Turkey. Engineering Structures. 2008.

[11] Inel, M., Ozmen, H. B., & Bilgin, H. (2008). Re-evaluation of building damage during recent earthquakes in Turkey. *Engineering Structure.*

[12] Inel, M., Senel, S. M., Toprak, S., & Manav, Y. (2008). Seismic risk assessment of buildings in urban areas: A case study for Denizli, Turkey. *Natural Hazards*.

[13] Dogan M, Unluoglu E, Ozbasaran H. Earthquake failures of cantilever projections buildings. Engineering Failure Analysis. 2007.

[14] Tezcan, S. S., & Alhan, C. (2001). Parametric analysis of irregular structures under seismic loading according to the new Turkish earthquake code. *Engineering Structures*.

[15] HODGES DH. Lateral-torsional flutter of a deep cantilever loaded by a lateral follower force at the tip. Journal of Sound and Vibration. 2001.

[16] WU, J.-J., & WHITTAKER, A. R. (1999). The natural frequencies and mode shapes of a uniform cantilever beam with multiple two-DOF spring–mass systems. *Journal of Sound and Vibration*.

[17] Zhou, D. (1997). The vibrations of a cantilever beam carrying a heavy tip mass with elastic supports. *Journal of Sound and Vibration*.

Appendices

Appendix A

Shell mesh and the mesh size

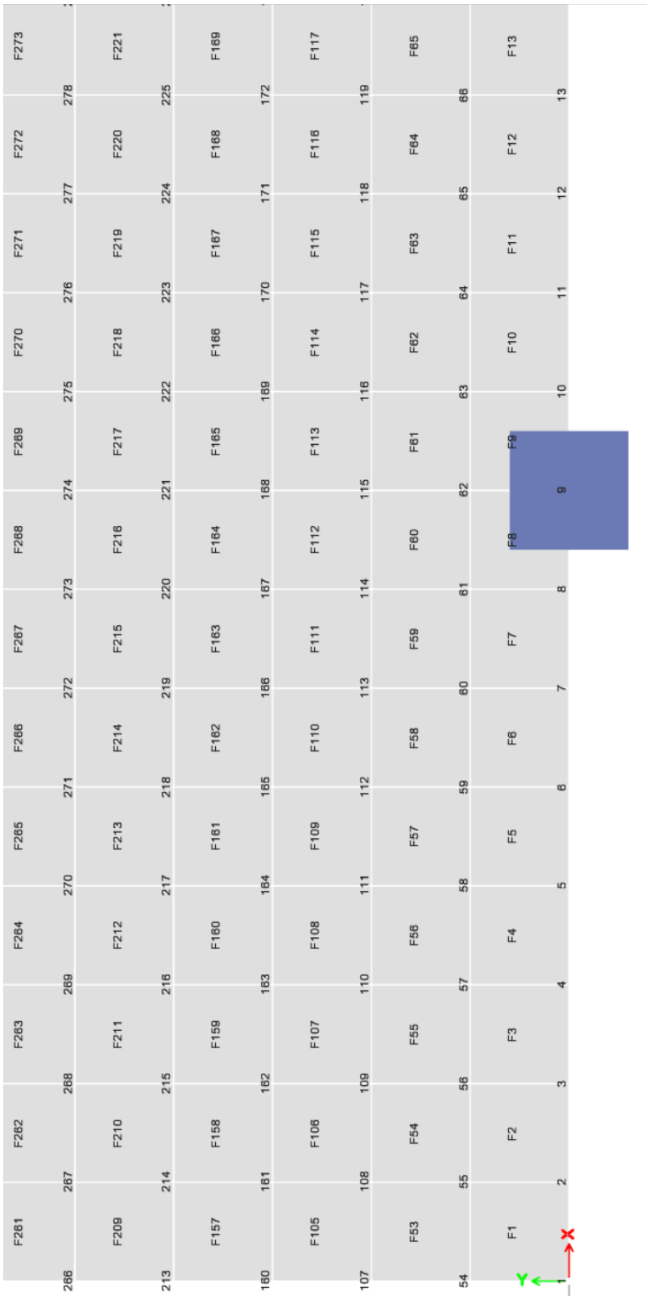

Appendix B

Applied Loads Calculations

Masonry wall load dead load applied to the slabs (SID)

Layers	Thickness(cm)	Unit weight(kN/m^3)	Weight(kN/mr)
stone	5	34	1.7
concrete	10	24	2.4
block	15	12.5	1.9
			6.0

Dead load applied to the slabs (SID)

Structural system	Slab thickness	Additional SID	Ribs block volume	Ribs block unit weight	Ribs block weight	Total SID
One way Ribbed slab	25	3	0.131	12.5	1.63	4.55
Two way ribbed slab	25	3	0.101	12.5	1.26	4.26

Appendix C

Design Parameters Calculations

calculation steps for the acceleration parameters of the design spectrum for the horizontal component in each city

city	zone	Z	Risk category	Importance factor	Ss	S1
Jericho	3	0.3	I	1	1.13	0.56
Nablus	2A	0.2	I	1	0.75	0.38
Hebron	2B	0.15	I	1	0.56	0.28
Beer Saba	1	0.075	I	1	0.28	0.14

city	Site class	Fa	Fv	Sms	Sm1	SDs	SD1
Jericho	D	1.05	1.7	1.18	0.96	0.79	0.64
Nablus	D	1.2	1.7	0.90	0.64	0.60	0.43
Hebron	D	1.35	1.74	0.76	0.49	0.51	0.33
Beer Saba	D	1.575	2.04	0.44	0.29	0.30	0.19

Appendix D

Static Design Results

The following figure shows the 3D model of 6 floors and the reinforcement steel results for dead and live loads.

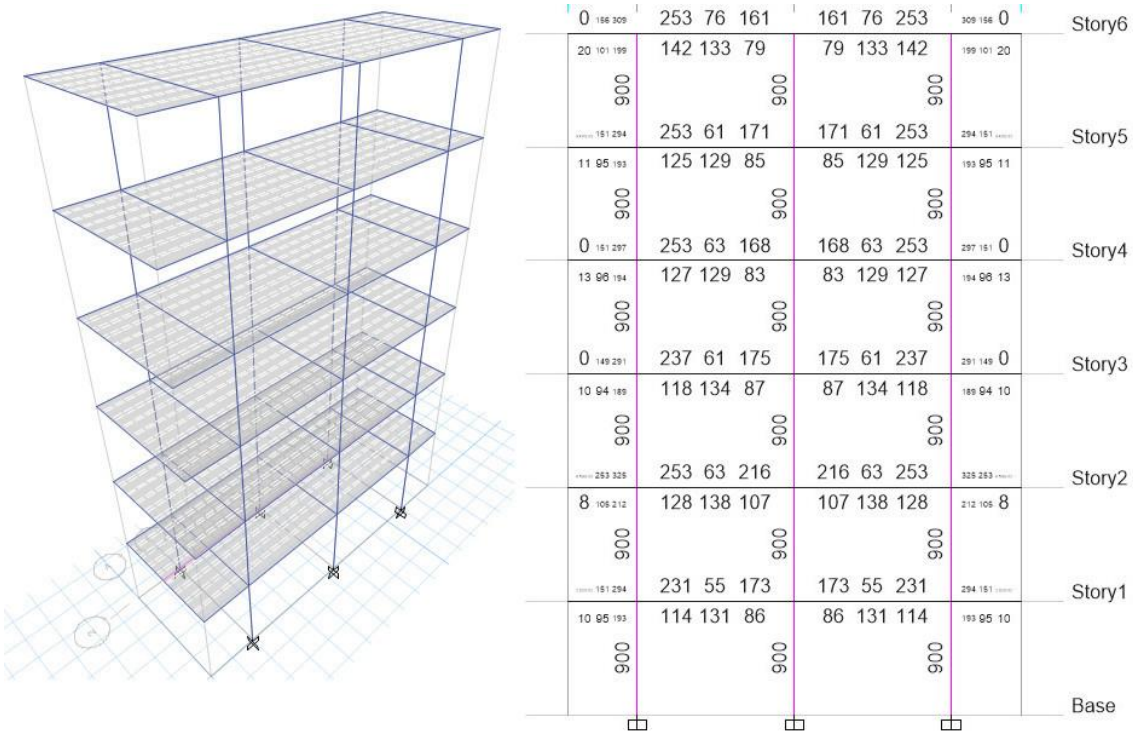

Appendix E

Diaphram Axial Load According To ASCE7-16

The following caption from the ASCE7-16 design code describes the limits of forces in the diaphragm, but it's not considered in the study because axial forces are calculated by multiplying weight by acceleration and not related to the codes.

$$F_{px} = \frac{\sum_{i=x}^{n} F_i}{\sum_{i=x}^{n} w_i} w_{px} \qquad (12.10\text{-}1)$$

where

F_{px} = the diaphragm design force at level x;
F_i = the design force applied to level i;
w_i = the weight tributary to level i; and
w_{px} = the weight tributary to the diaphragm at level x.

The force determined from Eq. (12.10-1) shall not be less than

$$F_{px} = 0.2 S_{DS} I_e w_{px} \qquad (12.10\text{-}2)$$

The force determined from Eq. (12.10-1) need not exceed

$$F_{px} = 0.4 S_{DS} I_e w_{px} \qquad (12.10\text{-}3)$$

Appendix F

Detailed Manual drawings for forces and stresses

Detailed Manual drawings for the axial force, shear force and bending moment diagrams:

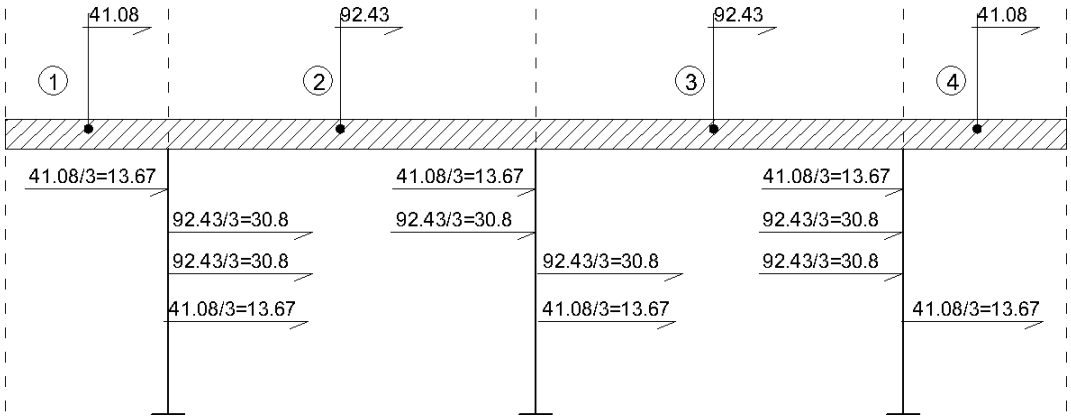

Axial force diagram due to first cantilever starting from left

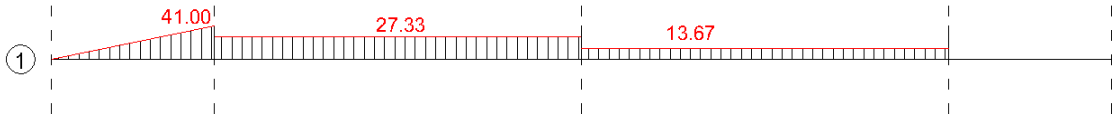

Axial force diagram due to first continues span starting from left

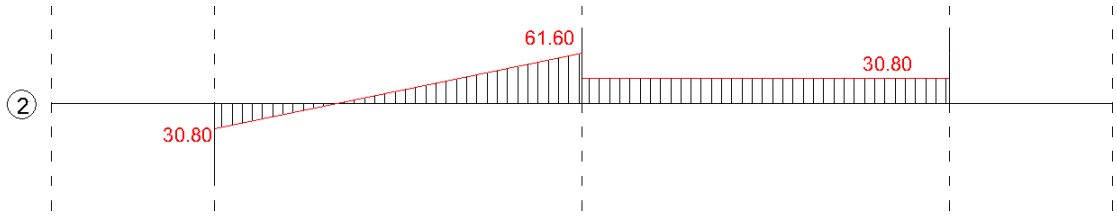

Axial force diagram due to second continues span starting from left

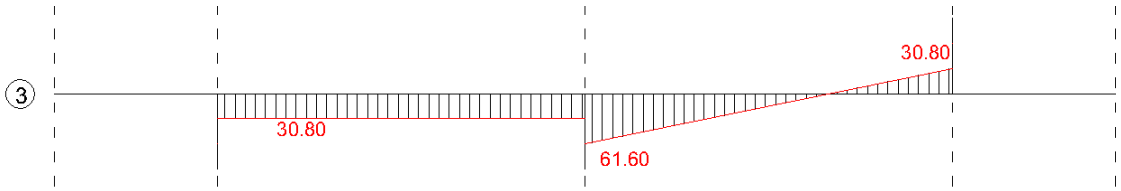

Axial force diagram due to end cantilever starting from left

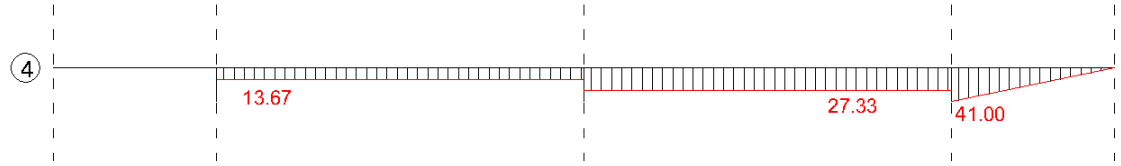

Total axial force diagram

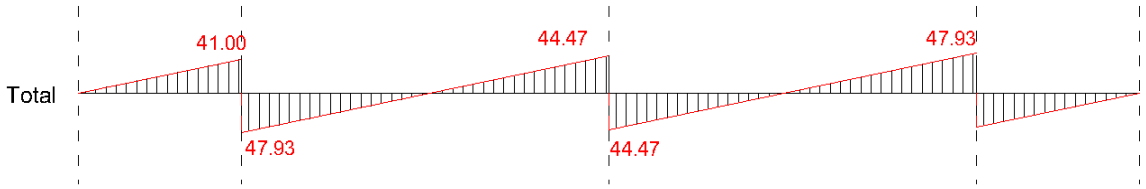

جـامعـــة النجاح الوطنية

كليـــة الدراســـات العليـــا

أثر المركبة الافقية للزلازل على الاسقف الطائرة المحملة بجدران ثقيلة

إعداد

معتز محمد ابراهيم ابو العدس

إشراف

د.عبد الرزاق طوقان

قدمت هذه الرسالة استكمالا لمتطلبات الحصول على درجة الماجستير في هندسة الإنشاءات، من كلية الدراسات العليا، في جامعة النجاح الوطنية، نابلس- فلسطين.

2022

أثر المركبة الافقية للزلازل على الاسقف الطائرة المحملة بجدران ثقيلة

اعداد

معتز محمد ابراهيم ابو العدس

إشراف

د.عبد الرزاق طوقان

الملخص

المقدمة: من الواضح جلياً ان معظم المباني المعاصرة تحتوي على طيرانات وفي معظم الحالات فإن هذه الطيرانات تكون محملة بجدران خارجية ثقيلة الى متوسطة الثقل، وكما هو متوقع فإن هذه الطيرانات اكثر عرضه للإنهيار تحت تأثير القواى الزلزالية، مما يؤدي الى ضعف الكفاءة الزلزالية للمنشأ بأكمله، وبما ان اثر المركبات الزلزالية على الطيرانات غير موصوف ومفصل بشكل واضح في كودات وكتب التصميم فهذا يشكل حاجة لبحوث في هذا المجال. في هذه الاطروحة سنتناول اثر المركبة الافقية للزلازل على الطيرانات المحملة والإستجابة الزلزالية لها. ان الهدف الاساسي لهذا البحث هو فهم التصرف الزلزالي للطيرانات عند تعرضها لمركبة زلزالية افقية تحت ظروف مختلفة وفي هذا البحث سيتم تناول بعض من اكثر خصائص الطيرانات حساسية وتأثيرا على التصرف الزلزالي لها للمساعدة على فهم اثرها على استجابة الطيرانات الزلزالية.

الطرق: تتمثل ألية البحث بعمل دراسة متقدمة تتضمن جمع وتحليل المعلومات حول خصائص الطيرانات ومؤثراتها مثل طول الطيران وحمله واتجاهه والموقع الجغرافي للمنشأ، ثم تكوين مجموعات من النماذج

التحليلية الانشائية المتشابهه في جميع الخصائص مع اختلاف في العامل المراد دراسته وتحليلها بإستخدام برنامج ايتابس (ETABS) بعد اعتماده والتأكد من دقة نتائجه.

النتائج: زادت نتائج القوى والعزوم الناتجة من المركبة الافقية للزلازل في وجود حال الجدران بنسبة 152٪ للقوى المحورية و 13.4٪ لقوى القص و العزم الدوراني. من ناحية أخرى ، المركبة العمودية للزلازل ليست الاكثر خطرا على المقاطع الكابولية, من ناحية اخري فإن اثر القوى المحورية الناجة من المركبة الافقية للزلازل على قدرة مقطع الكابولي لمقاومة قوى القصلم يتجاوز 2٪ للجسور و 1٪ للعقدات المعصبة, ويمكن ان تصل النسبة الحرجة لطول اللطيران نسبة لطول الخانة السابقة الى22% في بعض الحالات.

الخلاصة: يظهر البحث ان من الافضل تجنب المباني غير المنتظمة لتقليل عزوم الإلتواء قدر الامكان ,من ناحية اخرى فإن المباني المنتظمة والتي يتماثل فيها مركز الكتلة مع مركز الجسائة من الممكن ان يحدث فيها نموذج التواء مبكر. اظهر البحث ايضا ان المركبة الافقية للزلازل لاتحدث اثرا كبيرا على قدرة تحمل قوى القص للطيران كما واظهر ان المركبة العمودية ليست الاسوء تأثيرا على الطيرانات.

الكلمات المفتاحية: الطيرانات المحملة، الالتواء، المركبة الافقية للزلازل، المركبة الافقية للزلازل، زلزالية الموقع.